Published February 24, 2014

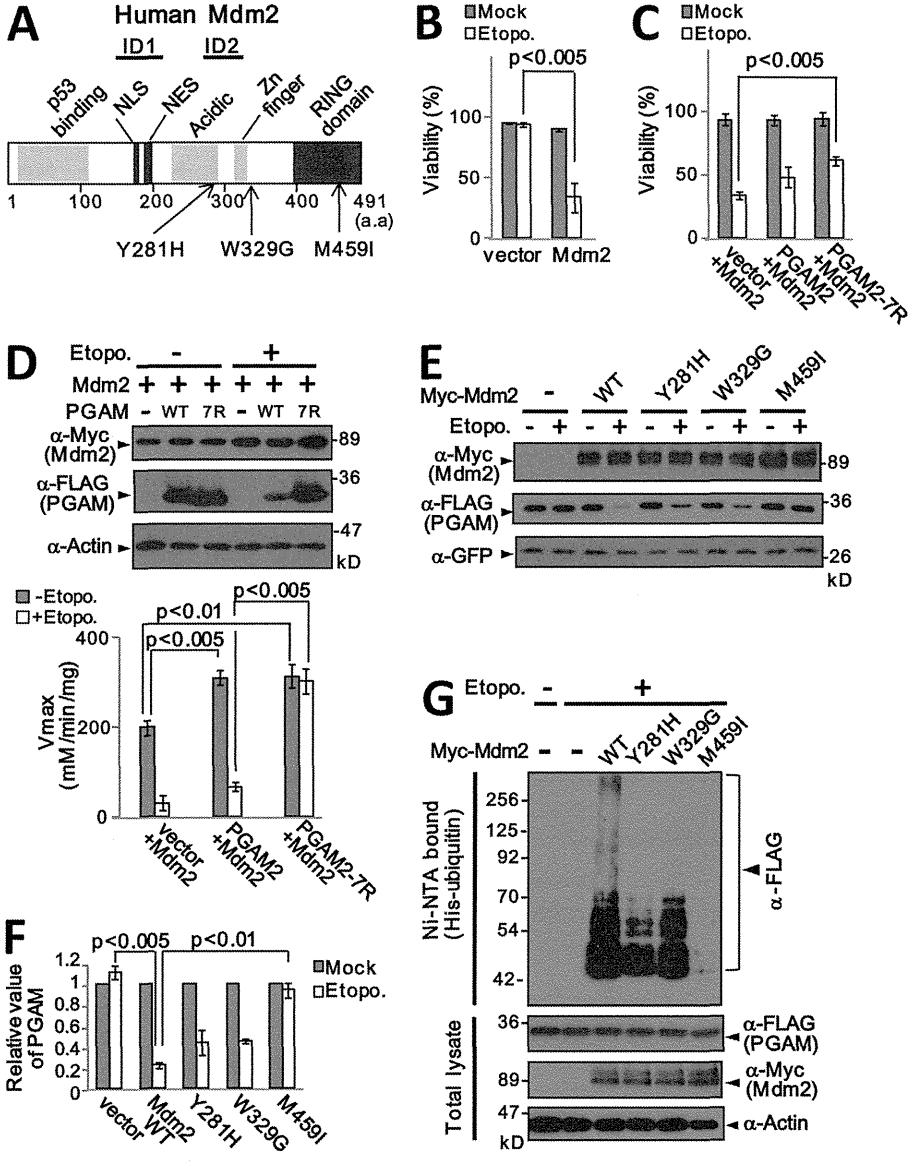

Figure 7. **Stabilization of PGAM by mutation of Mdm2 or PGAM retains cell viability.** (A) Schematic of the reported domain structure of Mdm2 and the location of cancer-associated mutations in human Mdm2 according to the COSMIC database. (B) Ectopic expression of Mdm2 reduces the viability of wild-type MEFs after DNA damage. Viable cells were counted by trypan blue staining. (C) The ability of PGAM2 variants to counteract the effects of Mdm2 and etoposide on cell viability. (D) Primary MEFs infected with vectors encoding Mdm2 and either PGAM2-WT-FLAG or PGAM2-7R-FLAG as indicated were treated with or without etoposide, and the levels of PGAM protein were assessed by immunoblotting (left). Samples of cell extract were also used to measure PGAM enzymatic activity (right). The viability of these cells is shown in C. (E) The ability of Mdm2 variants to restore PGAM2 protein levels after DNA damage. (F) Relative quantitation of the PGAM signal intensity in E normalized to that of GFP. (G) *p53*$^{-/-}$*Mdm2*$^{-/-}$ MEFs were cotransfected with His-ubiquitin, PGAM2-FLAG, and the indicated Mdm2 variants (WT, Y281H, W329G, or M459I). The cells were treated with or without etoposide, and cell extracts were analyzed by immunoblotting, either immediately (bottom) or after recovery of His-tagged ubiquitinated proteins on Ni-NTA agarose under denaturing condition (top). In B, C, D, and F, error bars indicate SEM (n = 3).

Collaboration between PGAM2, Mdm2, and Ras-G12V in cell transformation

Interestingly, the Y281H and M459I mutations in Mdm2, in glioma and lung carcinoma, respectively, were accompanied by activating mutations in the G12 residue of Ras (G12D and G12C). We therefore explored whether Ras-G12V and Mdm2 had cooperative effects on the proliferative potential of primary MEFs. Neither wild-type Mdm2 nor any of the three mutants (Y281H, W329G, and M459I) were able to immortalize Ras-G12V–expressing wild-type MEFs, whereas ablation of p53 with HPV E6 readily enabled the cells to bypass Ras-induced senescence (Fig. 8 A and Fig. S5 H). However, we obtained a strikingly different answer when these assays were performed using cells derived from a transgenic mouse line that we have developed, in which PGAM2-FLAG expression is driven by the *CAG* promoter (Niwa et al., 1991), a fusion between the cytomegalovirus immediate-to-early enhancer element and chicken *β-actin* promoters (Fig. 8 B). MEFs from the *PGAM*-Tg mice displayed enhanced glycolytic flux and lactate production (Fig. S5 I). When we infected the cells with Ras-G12V and the relevant mutants of Mdm2 (WT, Y281H, W329G, and M459I), and passaged them in a 3T3 protocol, the MEFs expressing Ras-G12V and Mdm2-M459I appeared to be immortal and were able to grow as anchorage-independent colonies in soft agar (Fig. 8, A, C, and D). The Mdm2 variants were expressed at equivalent levels shown by Western blotting (Fig. S5 J). Ubiquitination of PGAM protein was barely detectable in the *Ras-G12V/Mdm2-M459I/PGAM*-Tg MEFs, compared with the controls or cells transduced with the other Mdm2 mutants (Fig. 8 E and Fig. S5 K). Moreover, in the *Ras-G12V/Mdm2-M459I/PGAM*-Tg MEFs, both glycolytic flux and lactate production were upregulated (Fig. 8 F and Fig. S5 L).

We previously reported that MEFs expressing PGAM2 and Ras-G12V were unable to grow in soft agar (Kondoh et al., 2005), and, consistent with this observation, we found that Ras-G12V–expressing *PGAM2*-Tg MEFs could not form tumors in nude mice (Fig. 8 G). Of the cells expressing different Mdm2 variants, only the *Ras-G12V/Mdm2-M459I/PGAM*-Tg MEFs formed tumors in nude mice at a significant frequency (Fig. 8, G and H and Table 1). We presume that the M459I RING finger

Published February 24, 2014

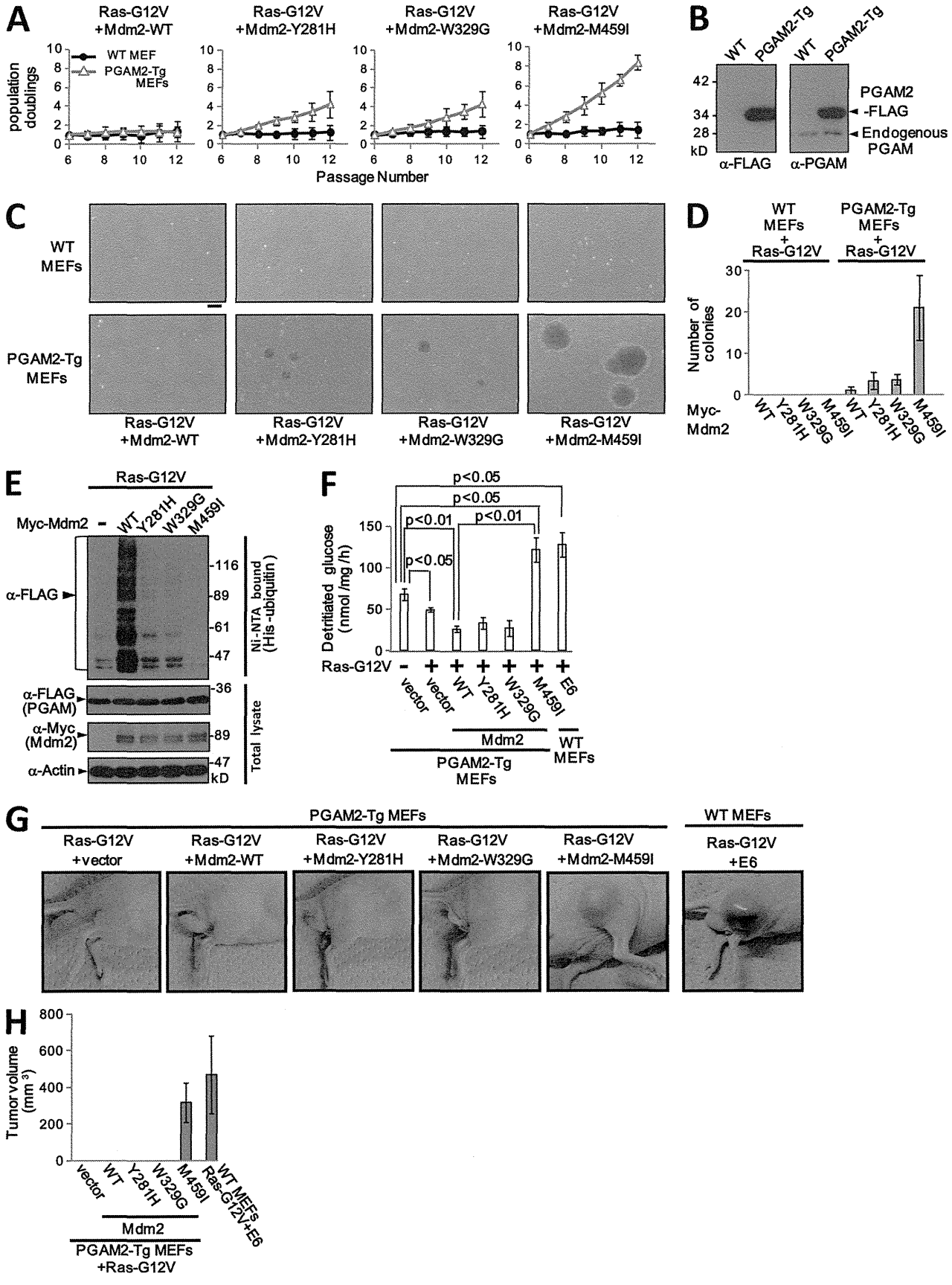

Figure 8. **Collaboration between PGAM2, Mdm2 and RasG12V in cell transformation.** (A) The ability of the indicated Mdm2 mutants to bypass RasG12V–induced senescence in *PGAM2*-Tg but not wild-type MEFs. (B) Relative levels of endogenous and FLAG-tagged PGAM2 in primary MEFs isolated from either wild-type or transgenic C57BL/6 mice that overexpress PGAM2-FLAG from the *CAG* promoter. Whole cell extracts of MEFs were analyzed

Published February 24, 2014

Table 1. **Formation of subcutaneous tumors in nude mice by PGAM2-Tg MEFs infected with Ras-G12V and various Mdm2 mutants**

Cells	Number tumors/number injected
PGAM2-Tg MEFs/*Ras-G12V* + vector	0/6
PGAM2-Tg MEFs/*Ras-G12V* + *Mdm2-WT*	0/12
PGAM2-Tg MEFs/*Ras-G12V* + *Mdm2-Y281H*	0/6
PGAM2-Tg MEFs/*Ras-G12V* + *Mdm2-W329G*	0/6
PGAM2-Tg MEFs/*Ras-G12V* + *Mdm2-M459I*	5/8
Wild-type MEFs/*Ras-G12V* + *E6*	6/6

Formation of subcutaneous tumors in nude mice after injection of *PGAM2*-Tg MEFs infected with the indicated expression vectors. For each injection, 5×10^6 cells were injected in a volume of 100 µl. Mice were sacrificed after 3 wk of monitoring. Representative results of two independent experiments are shown ($n = 2$).

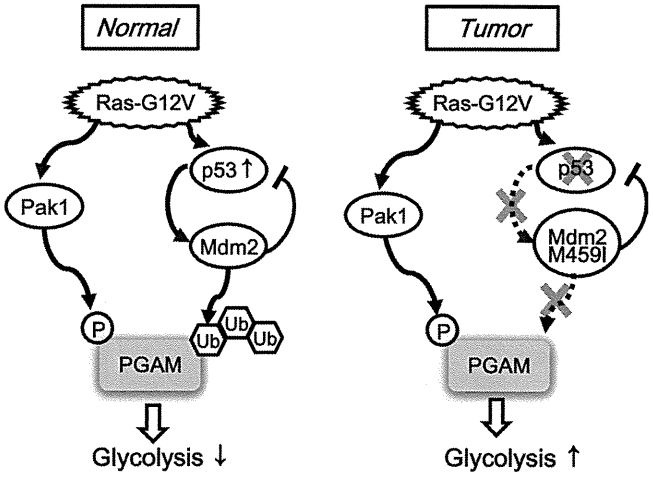

Figure 9. **Model.** Model for PGAM stabilization and effects on glycolysis in different cellular contexts. (left) In normal cells, Ras-G12V expression triggers PGAM ubiquitination associated with a decline of glycolysis via Pak1/Mdm2 activation. (right) The situation in tumors induced by Ras-G12V and Mdm2-M459I associated with stabilization of PGAM and enhanced glycolysis. Note that according to the International Cancer Genome Consortium (2010), missense mutations in Mdm2 are relatively rare, and only 2 of the 24 variants recorded thus far affect the RING domain.

mutation renders Mdm2 uniquely able to suppress p53 transactivation without destabilizing PGAM under stress conditions. Thus, in the context of activated Ras-G12V, our data imply that both Mdm2 and the glycolytic enzyme PGAM promote neoplastic transformation (Fig. 9).

Discussion

With the notable exception of PGAM, most glycolytic enzymes are transcriptionally regulated by HIF-1α (Iyer et al., 1998) or c-Myc (Osthus et al., 2000). Here we show that under conditions of DNA damage or oncogenic signaling, each of which provokes premature senescence in primary cells, PGAM is posttranscriptionally regulated through phosphorylation-dependent ubiquitination. Turnover of PGAM could account for the marked reduction of glycolytic flux observed in senescent cells, and the mechanistic insights we provide suggest a key role for the p53–Mdm2 axis in these events.

The first step in this process is the activation of Pak1 kinase, a direct downstream effector of Cdc42/Rac1 that is involved in many cellular processes, including cell motility, actin reorganization, gene transcription, and apoptosis, as well as in cancer (Molli et al., 2009). Amplification of the *Pak1* gene has been observed in human tumors (Schraml et al., 2003), whereas ectopic expression of Pak1 promotes hyperplasia in vivo (Wang et al., 2002) and cellular transformation in vitro (Vadlamudi et al., 2000). Moreover, mice that lack Merlin, an inhibitor of Pak1, display a cancer-prone phenotype that is exacerbated by p53 mutation (McClatchey et al., 1998). Here we reveal an unexpected role for Pak1 in cellular senescence in primary MEFs and human dermal fibroblasts exposed to various forms of stress. In this respect, the double-edged sword properties of Pak1 are reminiscent of those of oncogenic Ras-G12V, which elicits senescence in primary cells but cell proliferation and transformation in cells that evade senescence (Serrano et al., 1997).

Our findings also connect Pak1 to the regulation of glycolysis, as its involvement in senescence can be largely explained by its ability to phosphorylate PGAM on Ser118. We present several lines of evidence that in primary cells this event is critical for the subsequent ubiquitination and proteasome-mediated turnover of PGAM. PGAM is stabilized by shRNA-mediated depletion of Pak1 and by mutations that exclude phosphorylation by Pak1, whereas the corresponding phosphomimetic mutation promotes ubiquitination and turnover of PGAM.

Although we cannot discount the possibility that other ubiquitin E3 ligases might target PGAM, Mdm2 emerged as an obvious candidate based on the differential behavior of PGAM in p53-positive and -negative cells. We confirmed that phosphorylation of PGAM by Pak1 promotes the interaction between Mdm2 and PGAM under stress conditions, and that Mdm2 ubiquitinates PGAM in cultured cells and in vitro. The in vitro assays identified seven lysine residues in PGAM that are targets for Mdm2-mediated ubiquitination. Consistent with recent reports that ubiquitination sites are generally close to the preceding phosphorylation event (Hagai et al., 2012), the relevant lysine

by immunoblotting with anti-FLAG or -PGAM antibody. (C) Coexpression of the Mdm2-M459I mutant and Ras-G12V conferred anchorage-independent growth in *PGAM2*-Tg MEFs. Bar, 200 µm. (D) Anchorage-independent colonies in Fig. 8 C were counted after 3 wk. (E) The ability of the indicated Mdm2 variants to promote ubiquitination of PGAM2 in *PGAM2*-Tg/*Ras-G12V* MEFs. (F) Measurement of glycolytic flux in primary *PGAM2*-Tg MEFs expressing the indicated combinations of Ras-G12V and Mdm2 variants (WT, Y281H, W329G, or M459I). Wild-type MEFs expressing HPVE6 were used as a control. (G) *PGAM*-Tg MEFs (5×10^6 cells) expressing Ras-G12V and various mutants of Mdm2 (WT, Y281H, W329G, or M459I) were injected subcutaneously in nude mice, and tumor growth was monitored for 3 wk. Wild-type MEFs expressing Ras-G12V and E6 were used as a positive control. Representative photographs of mice in Table 1 are shown. In A, D, and F, error bars indicate SEM ($n = 3$). (H) Measurement of tumor volumes, which were shown in Table 1. Error bars indicate SEM.

Published February 24, 2014

residues in PGAM are located in the central domain, adjacent to the Pak1-phosphorylation site Ser118.

Mdm2 is known to ubiquitinate several other substrates, including the p53 tumor suppressor (Manfredi, 2010), and is therefore viewed as an oncogene. In line with this idea, amplification of the *Mdm2* gene has been observed in several human cancers (Leach et al., 1993; Reifenberger et al., 1993). It was also reported that the combination of Mdm2, oncogenic Ras-G12V, and adenovirus E1A will efficiently transform human primary fibroblasts (Seger et al., 2002). In contrast, we and others have noted that in primary cells, ectopic expression of wild-type Mdm2 induces cell cycle arrest (Brown et al., 1998) or apoptosis under conditions of stress (this paper). Moreover, whereas p53 ablation can rescue MEFs from Ras-G12V-induced senescence, ectopic expression of wild-type Mdm2 cannot.

The differential effects of cancer-associated Mdm2 mutants reveal a plausible explanation. Two of the mutations, Y281H and W329G, in the inhibitory domain 2 (ID2) of Mdm2 partly abolish its ability to ubiquitinate PGAM but not p53. The third mutation, M459I in the RING finger domain, completely abolishes ubiquitin ligase activity both for p53 and PGAM, while remaining able to block p53 transactivation. The relative potency of the Mdm2 mutants in PGAM ubiquitination closely correlated with their abilities to rescue PGAM-Tg MEFs from Ras-induced senescence. Strikingly, the combination of the M459I mutant of Mdm2 and oncogenic Ras-G12V was sufficient to transform primary MEFs from PGAM-Tg mice, but not those from wild-type mice. We suspect that this reflects the higher basal levels of glycolysis and lactate production in the PGAM-Tg, which would facilitate the bypassing of senescence. Collectively, the data suggest that in some contexts, Mdm2 might protect cells from transformation by promoting the ubiquitin-mediated turnover of PGAM. Alternatively, up-regulation of PGAM could promote the oncogenic effects of the mutant forms of Mdm2. Consistent with these ideas, the ubiquitination activity of Mdm2 is reported to be differentially regulated in a cellular context– and developmental stage–dependent manner (Itahana et al., 2007; Terzian et al., 2008).

Both enhanced glycolysis (the Warburg effect) and cellular immortalization are recognized as hallmarks of cancerous tissues and cells. Our data on the ubiquitination of PGAM by the p53/Mdm2 axis during SIS might partly explain how these hallmarks are coupled. The activation of p53 during senescence, whether via DNA damage or direct oncogenic signaling, would potentially down-regulate glycolytic flux by promoting Mdm2-mediated turnover of PGAM. Similar effects on glycolysis would be achieved via the transcriptional activity of p53 on other target genes, such as TIGAR and Glut3 (Bensaad et al., 2006; Kawauchi et al., 2008). Thus, p53 might function as a metabolic checkpoint against tumorigenesis partly by modulating the glycolytic pathway (Jones et al., 2005). As we have previously argued (Kondoh et al., 2005), the Warburg effect could represent a metabolic adaptation that enables incipient cancer cells to evade senescence.

Several recent studies have emphasized the importance of PGAM as a therapeutic target for cancer management (Durany et al., 1997, 2000, Evans et al., 2005; Vander Heiden et al., 2010; Hitosugi et al., 2012). Our identification of physiological modulators of PGAM stability might open up new avenues for therapeutic intervention.

Materials and methods

Cell culture

Primary MEFs were isolated from 13.5-d postcoitum embryos of C57BL6 mice as described previously (Carnero et al., 2000). The head and blood organs of embryos were removed, and the torso was placed on a 10-cm plate. The embryo was minced with a scalpel and dispersed in 0.1% trypsin (45 min at 37°C). Cells were grown for two population doublings, followed by retroviral infection or transfection of plasmids. Human primary fibroblast (IMR90, WI-38, and TIG3), human immortalized cell lines (HeLa, 293T, HCT116, RKO, HT-29, and SW620), primary MEFs from *p53*$^{-/-}$, *p53*$^{-/-}$*Mdm2*$^{-/-}$, and *PGAM2*-Tg mice were grown in DMEM with 10% FBS. *PGAM2*-Tg is a strain of transgenic C57BL/6 mice that overexpress PGAM2 under the cytomegalovirus immediate-to-early enhancer element and chicken *β-actin* promoter (*CAG*). The GFP-tagged p53-inducible cell line, TGP53-4, was grown with or without 1 μM doxycycline. To model SIS, primary cells were exposed to 20 μM etoposide.

Transfection, retroviral infection, and SA-β-gal staining

Transfection was performed by using Fugene-HD (Roche) or the calcium phosphate transfection method (Kondoh et al., 2005). EcoPack2-293 (Takara Bio Inc.) packaging cell lines were used for retroviral production. Infected cells were selected by the addition of 75 μg/ml hygromycin, 400 μg/ml (G418), or 2 μg/ml puromycin, as appropriate for the vector. After drug selection, cultures were propagated according to a 3T3 protocol as described previously (Carnero et al., 2000). Cytochemical staining for SA-β-gal was performed at pH 6.0, as described previously (Dimri et al., 1995). The percentage of SA-β-gal–positive cells was determined microscopically by counting the number of positive-staining cells among over 200 cells in total. Images were recorded using a microscope (BZ-9000; KEYENCE) using a 10× 0.45 NA Plan-Apochromat objective lens.

Viability assay

Primary MEFs transfected with various combinations of expression vectors were grown for 24 h and treated with 50 μM etoposide for 24 h. Cells were then collected and stained by trypan blue. Viable cells were counted using a light microscope.

Immunoblotting assay and RNA analysis

For immunoblotting, cell lysates were prepared 24 h after transfection as described previously (Carnero et al., 2000). Cells were washed twice with ice-cold PBS and lysed in lysis buffer (50 mM Tris-HCl, pH 7.5, 200 mM NaCl, 1 mM EDTA, 10% glycerol, 0.5% Triton X-100, 50 mM NaF, 1 mM DTT, 1 mM Na_3VO_4, 1 mM phenylmethanesulfonyl fluoride, and protease inhibitor cocktail; Sigma-Aldrich). After 30 min on ice, lysates were vortexed and cleared by centrifugation. Equivalent amounts of protein were resolved by SDS-PAGE. The antibodies used for immunoblotting and immunostaining are described in the Recombinent proteins and antibodies section.

Total RNA was prepared using the TRIzol reagent (Invitrogen), and cDNA pools were generated using an oligo-dT primer (Promega) and SuperScript III reverse transcription (Invitrogen). Semiquantitative RT-PCR was performed by using a SuperScript one-step RT-PCR kit (Invitrogen) as described previously (Carnero et al., 2000), and real-time PCR was performed using Fast Start Universal SYBR Green Master (Roche). The primers used in these analyses are presented in the Primers section.

Immunoprecipitation

For immunoprecipitation assays, cell lysates were precipitated with the relevant antibody for 2 h. Immune complexes recovered with protein G–agarose beads were washed four times with lysis buffer (50 mM Tris-HCl, pH 7.5, 200 mM NaCl, 1 mM EDTA, 10% glycerol, 0.5% Triton X-100, 50 mM NaF, 1 mM DTT, 1 mM Na_3VO_4, 1 mM phenylmethanesulfonyl fluoride, and protease inhibitor cocktail; Sigma-Aldrich) and boiled in 2× Laemmli sample buffer for 5 min. Denatured immune complexes were resolved on SDS-polyacrylamide gels.

Ubiquitination assays

For detection of ubiquitinated forms of endogenous PGAM, cell extracts were immunoprecipitated with an anti-PGAM antibody, and the precipitated

Published February 24, 2014

proteins were denatured and resolved by SDS-PAGE. Ubiquitinated proteins were detected by immunoblotting with an antibody (clone FK2) that detects mono- and polyubiquitinated conjugates.

Detection of proteins labeled with His-tagged ubiquitin was performed as described previously, with modifications (Li et al., 2003). Cells were generally cotransfected with 3 µg of PGAM-FLAG expression plasmid and 3 µg of CMV-driven His-ubiquitin expression plasmid (a gift from T. Matsusaka, The Gurdon Institute, University of Cambridge, Cambridge, UK). After 24–36 h, cells were treated with either 20 µM etoposide for 6 h or exposed to other forms of stress (e.g., Ras-G12V) and treated with MG132. After harvesting, 10% of the cells were processed for direct analysis by immunoblotting while the remainders were used for purification of His-tagged ubiquitinated proteins.

Cell extract was prepared in denaturing conditions by using 6 M guanidine hydrochloride. Cells were resuspended in guanidine lysis buffer (6 M guanidine hydrochloride, 10 mM Tris-Cl, 100 mM Na_2HPO_4, 150 mM NaCl, 0.1% NP-40, and 20 mM imidazole, pH 8.0) at room temperature and sonicated. The lysate was centrifuged at 14,000 *g* for 10 min, and the supernatant was incubated with Ni-NTA beads (QIAGEN) for 2 h at room temperature. The beads were washed five times with guanidine wash buffer (6 M guanidine hydrochloride, 10 mM Tris-Cl, 100 mM Na_2HPO_4, 150 mM NaCl, 0.1% NP-40, and 20 mM imidazole, pH 6.3) at room temperature, followed by five cycles with ice-cold guanidine-free wash buffer (10 mM Tris-Cl, 100 mM Na_2HPO_4, 150 mM NaCl, 0.1% NP-40, and 20 mM imidazole, pH 6.3). His-tagged proteins were eluted from the beads with 50 µl of elution buffer (10 mM Tris-Cl, 100 mM Na_2HPO_4, 150 mM NaCl, 0.1% NP-40, and 250 mM imidazole, pH 6.3). Eluted fractions were analyzed by SDS-PAGE. Ubiquitinated PGAM2-FLAG protein was detected by immunoblotting with anti-FLAG antibody (M2).

In vitro ubiquitination assay

The following GST-tagged recombinant proteins were expressed and purified from *Escherichia coli*: GST-Mdm2-WT, GST-Mdm2-Y281H, GST-Mdm2-W329G, GST-Mdm2-M459I, GST-Mdm2-C464A, GST-p53, GST-PGAM2-WT-FLAG, GST-PGAM2-T2-FLAG, GST-PGAM2-T2-7R-FLAG, GST-PGAM2-TN-FLAG, GST-PGAM2-T4-FLAG, and GST-PGAM2-TC-FLAG. The GST tags were removed from GST fusion proteins by PreScission Protease (GE Healthcare). Other recombinant proteins were purchased: E1 enzyme (UBE1; Boston Biochem), His_6-tagged E2 enzyme (UbcH5b; Enzo Life Sciences), and His_6-tagged ubiquitin (EMD Millipore). In vitro ubiquitination reactions were performed as previously described with some modifications (Li et al., 2003). 35 ng PGAM2-FLAG or p53 was mixed with 100 ng UBE1 (E1), 500 ng UbcH5b (E2), His_6-tagged ubiquitin, and 500 ng Mdm2 (E3). These components were incubated in 30 µl of RXB buffer (40 mM Tris-HCl, pH 7.5, 5 mM $MgCl_2$, 10 mM NaCl, 1 mM DTT, and 2 mM MgATP) for 90 min at 37°C. The ubiquitinated proteins were analyzed by SDS-PAGE and detected by immunoblotting with anti-FLAG (M2) or anti-p53 (DO-1) antibody, respectively.

In vitro kinase assay

Primary MEFs were treated with 20 µM etoposide for 6 h, then lysed with lysis buffer. Endogenous Pak1 proteins were immunoprecipitated from the cell lysates with an anti-Pak1 antibody, and the precipitated proteins were washed twice with Pak1 kinase buffer (100 mM Hepes, 20 mM $MgCl_2$, 4 mM $MnCl_2$, and 0.4 mM dithiothreitol). Equivalent amounts of precipitated protein were incubated with 5 µg of recombinant PGAM2-WT or PGAM2-S118C in 30 µl of Pak1 kinase buffer for 30 min at 30°C in the presence of 10 µCi of γ-[^{32}P]ATP and 10 mM cold ATP. The labeled products were subsequently resolved by SDS-PAGE.

Cycloheximide chase assay

Primary MEFs were cotransfected with plasmids encoding PGAM2-FLAG (WT or S118C mutant) and GFP protein. Transfected cells were treated with 25 µM cycloheximide for 0–120 min. Subsequently, the levels of PGAM2-FLAG and GFP protein were determined by immunoblotting (Ogawara et al., 2002).

Measurement of PGAM activity

PGAM catalytic activity was measured spectrophotometrically as described previously (Kondoh et al., 2005). In brief, samples (20 µg) of cell lysate were incubated with 0.2 mM NADH, 3 mM ADP, 10 µM 2,3-diphosphoglycerate, 600 mU lactate dehydrogenase, 500 mU pyruvate kinase, and 100 mU enolase at 37°C for 10 min. 3-phosphoglyceric acid (3-PGA; 1 mM final concentration) was then added as a substrate. Activity was measured as NAD^+ release over 45 min by monitoring the decrease in absorbance at 340 nm in a Spectra max spectrophotometer (Molecular Devices).

Glycolytic flux measurement

The method used to determine glycolytic flux was based on the metabolism of D-[3-^{3}H] glucose into water after the triose phosphate isomerase reaction. Cells were plated at 0.7 × 10^6 cells per 100-mm dish, and the medium was changed from high glucose (17 mmol/liter) to low glucose (4.25 mmol/liter) 11 h later. D-[3-^{3}H] glucose was added 10 h later. Every 2 h, samples (400 µl) of medium were taken and precipitated with perchloric acid. The supernatant was applied to DOWEX 1X8 200-400 MESH Cl (Sigma-Aldrich) resin after dilution in sodium tetraborate, and the amount of [^{3}H] water in the flow-through was normalized to protein content. Lactate concentration in the culture medium was measured by the lactate assay kit (BioVision), and the value of lactate production was normalized to the protein content of the corresponding cell lysate.

Detection of γ-H2AX foci

Cells plated on coverslips were pre-permeabilized in 0.1% Triton buffer (0.1% [vol/vol] Triton X-100, 20 mM Hepes-KOH, pH 7.4, 50 mM NaCl, 3 mM $MgCl_2$, and 300 mM sucrose) and fixed with 3.7% paraformaldehyde in PBS. The cells were permeabilized with 0.5% Triton buffer (0.5% [vol/vol] Triton X-100, 20 mM Hepes-KOH, pH 7.4, 50 mM NaCl, 3 mM $MgCl_2$, and 300 mM sucrose), followed by treatment with blocking buffer (0.1% skim milk and 0.1% BSA in PBS) and primary antibody solution (anti–γ-H2AX phospho-Ser139 antibody in blocking buffer). After washing with PBS, the coverslips were treated with secondary antibody solution (Alexa Fluor 488 in blocking buffer). Nuclei were stained with DAPI. Images were recorded using a fluorescence microscope (BZ-9000; KEYENCE), using a 40× NA 0.95 Plan-Apochromat objective lens.

Luciferase reporter assay

p53$^{-/-}$*Mdm2*$^{-/-}$ MEFs were transfected with plasmids containing the p21^{CIP1}, Mdm2, or Bax promoter regions upstream of the firefly luciferase reporter in the pGL3 vector (Samuels-Lev et al., 2001), with or without a plasmid encoding wild-type p53, and a renilla luciferase plasmid (pRL-SV40) as a control for transfection efficiency. Cells were harvested 30 h after transfection, and the firefly and renilla luciferase activities were measured using a Dual-Glo Luciferase Assay System (Promega) and a luminometer (Lumat LB9507; BERTHOLD). The levels of firefly luciferase activity were normalized to those of renilla activity.

Soft agar assay

Soft agar assays were performed as described previously (Serrano et al., 1996). Culture dishes (6 cm) were prepared with a bottom layer of 3 ml of DMEM containing 0.4% low-melting agarose. 10^4 cells were mixed with 4 ml of DMEM containing 0.3% low–melting point agarose and seeded on the bottom layer. The colonies were allowed to grow for 2–3 wk and counted by light microscopy.

Nude mouse xenograft assays

8-wk-old nude mice (CAnN.Cg-*Foxn*^{nu}/CrlCrlj; Charles River Laboratories) were injected subcutaneously with 5 × 10^6 cells suspended in 100 µl PBS. Tumor formation was assessed after 3 wk. The procedures for performing animal experiments were in accordance with the principles and guidelines of the Animal Care and Use Committees of Kyoto University Graduate School of Medicine.

Recombinant proteins and antibodies

GST recombinant proteins were expressed in bacteria using pGEX6p-based plasmids. The proteins were purified on glutathione-agarose beads using standard protocols, and the GST tag was removed from the fusion proteins by treatment with PreScission Protease (GE Healthcare). Two rabbits were inoculated with full-length recombinant PGAM2 and the resultant antisera were affinity-purified by reactivity with the recombinant PGAM2.

A phospho-specific antibody against Ser118 of PGAM2 (anti-phospho S118) was generated by injecting rabbits with different synthetic phospho-peptides—B-118P (CVKIWRRS(PO_3)YDVP) and M-118P (CVKIWRRS(PO_3)FDTP)—conjugated to keyhole limpet hemocyanin (KLH) as an adjuvant. Antiserum from one of the four rabbits was found to recognize both phospho-peptides, B-118P and M-118P, but not the unphosphorylated peptides (Fig. S2 A). This rabbit antiserum was affinity purified on an immobilized phospho-peptide column (Thorslund et al., 2007).

Other antibodies used in this study were as follows: anti-FLAG (M2, F3165) from Sigma-Aldrich; anti-HA (12CA5) and anti-GFP from Roche; anti–c-Myc (9E10), anti-actin (C-11), anti-Pak1 (N-20), anti–human p53 (DO-1), anti-p21^{CIP1} (C-19), and anti-p16^{INK4} (M156) from Santa Cruz Biotechnology, Inc.; anti–mouse p53 (pAb421) from EMD Millipore; anti-Mdm2

Published February 24, 2014

(2A10) and anti-PGK from Abcam; anti-GAPDH (6C5) from EMD Millipore; anti-Enolase from BD; anti-PFK (C-terminal L684) from Abgent; anti-phospho Ser1981 ATM (10H11.E12) from Rockland Immunochemicals Inc.; anti–γ-H2AX (phosphor-Ser139 antibody; ab2893) from Abcam; Alexa Fluor 488 (A11070) from Invitrogen; and anti–mono- and polyubiquitinated conjugates antibody (clone FK2) from Enzo Life Sciences.

Plasmid DNAs

pHygro Marx II retroviral vectors encoding mouse *PGAM1* or *PGAM2* have been described previously (Kondoh et al., 2005). Expression of full-length *PGAM1* and *PGAM2* with no tag was driven by retroviral LTR promoter of pHygro Marx II. Human *PGAM1* cDNA was generated by RT-PCR from cell RNA and cloned into the pWZL neo retroviral vector. The human PGAM2 expression plasmid was a gift from Y. Yoshida (Center for iPS Cell Research and Application [CiRA], Kyoto University, Kyoto, Japan). Site-directed mutations in *PGAM2* were generated by PCR-based mutagenesis as described previously. The relevant variants of *PGAM2* are as follows: PGAM2-S118C, PGAM2-S118D, PGAM2-S118A, PGAM2-4R, and PGAM2-7R. Deletion mutants of mouse *PGAM2* cDNA were also generated by PCR, including PGAM-T1, PGAM-T2, PGAM-T3, PGAM-TN, PGAM-T4, and PGAM-TC. The different variants of *PGAM2* cDNA, and the wild-type PGAM1-WT and PGAM2-WT, were subcloned into the p3×FLAG-CMV14 expression vector. To produce recombinant proteins in bacteria, wild-type *PGAM2* and the PGAM2-S118C mutant cDNAs were transferred into the pGEX6p expression vector. HA-tagged *Pak1* cDNA was subcloned into a retroviral WZL-neo vector. The kinase-defective mutant Pak1-K299R (Zhang et al., 1995) was generated by PCR-based mutagenesis. To produce shRNAs against mouse *Pak1*, the relevant DNA oligonucleotides were annealed and ligated into the HindIII and BglII sites of the pRETRO-SUPER vector (Oligoengine; Brummelkamp et al., 2002). The pCMV-Myc vector containing human *Mdm2* cDNA has been described previously. Substitution mutants of *Mdm2* (Y281H, W329G, M459I) were generated by PCR-based mutagenesis. The CMV-driven human Mdm2 C464A expression plasmid was a gift from K.H. Vousden (Cancer Research UK, Beatson Institute, London, England, UK). The variants of *Mdm2* cDNA were cloned into the pCMV-Myc vector or the WZL-neo retroviral vector. For the in vitro ubiquitination assay, the variants of 3×FLAG-tagged *PGAM2* cDNA, including PGAM2-T2, -T2-7R, -TN, -T4, and -TC, were subcloned into the pGEX6p vector. Similarly, the various forms of human *Mdm2* (WT, Y281H, W329G, M459I, and C464A) and *p53* were subcloned into pGEX6p. The pBabe-puro-Ras-G12V plasmid was a gift from K. Maehara (National Center for Child Health and Development, Tokyo, Japan). To generate *PGAM2* transgenic mice, FLAG-tagged *PGAM2* was cloned into the pCAGGS vector. The pGAGGS plasmid was a gift from J.-i. Miyazaki (Division of Stem Cell Regulation Research, Osaka University Graduate School of Medicine, Osaka, Japan). The primer sequences used in this study are presented below.

cDNA

Accession numbers of cDNA (available from GenBank) used in this study were as follows: mouse *PGAM1*, NM_023418; mouse *PGAM2*, NM_018870; human *PGAM1*, NM_002629; human *PGAM2*, NM_013016; rat *Pak1*, NM_017198; human *Mdm2*, NM_00239.5.

Primers used for subcloning of *PGAM1* (PGM-B) and *PGAM2* (PGM-M) cDNA. PGM-M forward (Fw), 5′-AAGAATTCATGACCACCCACCGCCTAG-3′; PGM-M reverse (Re), 5′-ATATGGATCCTGGCTTCGCCTTTCCCTGGGCA-3′; PGM-B Fw, 5′-ATATGAATTCATGGCTGCCTACAAGCTGGT-3′; PGM-B Re, 5′-ATATGGATCCTGGCTTCTTCACCTTGCCCTGAG-3′; hPGM-B Fw, 5′-ATATGGGATCCGCCACCATGGCCGCCTACAAACTGGTG-3′; hPGM-B Re, 5′-ATATGAATTCTCACTTCTTGGCCTTGCCCTGG-3′.

Primers used for mutagenesis of *PGAM2* cDNA. PGM-M Fw, 5′-AAGAATTCATGACCACCCACCGCCTAG-3′; PGM-M Re, 5′-ATATGGATCCTGGCTTCGCCTTTCCCTGGGCA-3′; S118C Fw (mutation site F), 5′-CAGGTGAAGATCTGGAGGCGTTGCTTTGACACCCCACCACCACCC-3′; S118C Re (mutation site R), 5′-GGGTGGTGGTGGGGTGTCAAAGCAACGCCTCCAGATCTTCACCTGCTC-3′; S118A Fw (mutation site F), 5′-CAGGTGAAGATCTGGAGGCGTGCCTTTGACACCCCACCACCACCC-3′; S118A Re (mutation site R), 5′-GGGTGGTGGTGGGGTGTCAAAGGCACGCCTCCAGATCTTCACCTG-3′; S118D Fw (mutation site F), 5′-CAGGTGAAGATCTGGAGGCGTGACTTTGACACCCCACCACCACCC-3′; S118D Re (mutation site R), 5′-GGGTGGTGGTGGGGTGTCAAAGTCACGCCTCCAGATCTTCACCTGCTC-3′; 4R-1 Fw (mutation site F), 5′-CCATGGAAGAGAAACACAACTACTACACCTCCATCAGCAGGGACCGC-3′; 4R-1 Re (mutation site R), 5′-GCGGTCCCTGCTGATGGAGGTGTAGTAGTTGTGTTTCTCTTCCATGG-3′; 4R-2 Fw (mutation site F), 5′-GAGACGGCTGCAAGGCACGGGGAGGAGCAGGTGAGGATCTGGAGGCG-3′; 4R-2 Re (mutation site R), 5′-CGCCTCCAGATCCTCACCTGCTCCTCCCCGTGCCTTGCAGCCGTCTC-3′; 7R-1 Fw (mutation site F), 5′-GTGGCCTCACAGGCCTCAATAGGGCTGAGACGGCTGCAAGGCACGGG-3′; 7R-1 Re (mutation site R), 5′-CCCGTGCCTTGCAGCCGTCTCAGCCCTATTGAGGCCTGTGAGGCCAC-3′; 7R-2 Fw (mutation site F), 5′-GGCTTGAGGCCTGAGGAGCTGCCTACCTGTGAAAGTCTCAGGGACAC-3′; 7R-2 Re (mutation site R), 5′-GTGTCCCTGAGACTTTCACAGGTAGGCAGCTCCTCAGGCCTCAAGCC-3′.

Primers used to generate deleted versions of *PGAM2* cDNA. Pgam2F, 5′-CCGAATTCATGACCACCCACCGCCTAGT-3′; F1, 5′-CCGAATTCATGGTGGTGCGTACCTGGC-3′; R1, 5′-CCGATATCCTTCGCCTTTCCCTGGGCAGC-3′; F2, 5′-CGGAATTCATGAAGATTAAGGCTGCCAGAGAG-3′; R2, 5′-CCGATATCAGGTGCGATCTCCTCATTCC-3′; R3, 5′-GTGATATCGGGCACCCACACATTTGGTC-3′. Pgam2F and R1 were used for PCR of PGAM2-T1 cloning. F1 and R1 were used for PCR of PGAM2-T2 cloning. Pgam2F and R2 were used for PCR of PGAM2-T3 cloning. Pgam2F and R3 were used for PCR of PGAM2-TN cloning. F1 and R2 were used for PCR of PGAM2-T4 cloning. F2 and R1 were used for PCR of PGAM2-TC cloning.

Primers used for mutagenesis of *Mdm2* cDNA. Mdm2 Fw (mutation site F), 5′-ATAGAATTCTGGTGAGGAGCAGGCAA-3′; Mdm2 Re (mutation site R), 5′-TATCTCGAGCTAGGGGAAATAAGTTAGCAC-3′; Y281H Fw (mutation site F), 5′-GATGAGGTATATCAAGTTACTGTGCATCAGGCAGGGGAGAGTGATAC-3′; Y281H Re (mutation site R), 5′-GTATCACTCTCCCCTGCCTGATGCACAGTAACTTGATATACCTCATC-3′; W329G Fw (mutation site F), 5′-GATGTTGGGCCCTTCGTGAGAATGGGCTTCCTGAAGATAAAGGGAAAG-3′; W329G Re (mutation site R), 5′-CTTTCCCTTTATCTTCAGGAAGCCCATTCTCACGAAGGGCCCAACATC-3′; M459I Fw (mutation site F), 5′-CATGGCAAAACAGGACATCTTATTGCCTGCTTTACATGTGCAAAGAAG-3′; M459I Re (mutation site R), 5′-CTTCTTTGCACATGTAAAGCAGGCAATAAGATGTCCTGTTTTGCCATG-3′.

Primers used for mutagenesis of *Pak1* cDNA. Pak1 Fw (mutation site F), 5′-ATATGAATTCACCATGTACCCATACGACGTG-3′; Pak1 Re (mutation site R), 5′-ATATGAATTCTCAGTGATTGTTCTTGGTTGCC-3′; K299R Fw (mutation site F), 5′-ACAGGGCAGGAGGTGGCCATTAGACAGATGAACCTTCAGCAGCAG-3′; K299R Re (mutation site R), 5′-CTGCTGCTGAAGGTTCATCTGTCTAATGGCCACCTCCTGCCCTGT-3′.

Primers used to generate *Pak1* shRNA. shPak1 no. 1 Fw, 5′-GATCCCCGTACACACGGTTCGAGAAGTTCAAGAGACTTCTCGAACCGTGTGTACTTTTTTGGAAA-3′; shPak1 no. 1 Re, 5′-AGCTTTTCCAAAAAGTACACGGTTCGAGAAGTCTCTTGAACTTCTCGAACCGTGTGTACGGG-3′; shPak1 No. 2 Fw, 5′-GATCCCCCCCCTAAACCAGGGCTCCAATTCAAGAGATTGGAGCCGTGGTTTAGGGTTTTTGGAAA-3′; shPak1 No. 2 Re, 5′-AGCTTTTCCAAAAACCCTAAACCACGGCTCCAATCTCTTGAATTGGAGCCGTGGTTTAGGGG-3′.

Primers used to generate the *PGAM2* transgene in mice. Forward, 5′-ATATGAATTCATGACCACCCACCGCCTAGT-3′; reverse, 5′-ATATGAATTCCTACTTGTCATCGTCATCCT-3′.

Primers used for semi-quantitative RT-PCR. Mouse PGAM1 Fw, 5′-GAACTGTGCTGTGGTGTGACC-3′; mouse PGAM1 Re, 5′-AGCTCTGAACCCACACGGTAG-3′; mouse PGAM2 Fw, 5′-GGCTTGAAGCCTGAGGAGCTG-3′; mouse PGAM2 Re, 5′-AACTTTATTGCCCCGTCCACC-3′; mouse β-actin Fw, 5′-AGGCTCTTTTCCAGCCTTCCT-3′; mouse β-actin Re, 5′-ATAAGAGACAACATTGGCATGGC-3′.

Primers used for real-time qRT-PCR analysis. Mouse PGAM1-qRT Fw, 5′-GTTGCGAGATGCTGGCTATGA-3′; mouse PGAM1-qRT Re, 5′-CACATCTGGTCAATGGCATCC-3′; mouse PGAM2-qRT Fw, 5′-TGGAATGAGGAGATCGCACCT-3′; mouse PGAM2-qRT Re, 5′-TCGGACATCCCTTCCAGATGT-3′; mouse β-actin-qRT Fw, 5′-CGTGCGTGACATCAAAGAGAA-3′; mouse β-actin-qRT Re, 5′-AACCGCTCGTTGCCAATAGT-3′; mouse Mdm2-qRT Fw, 5′-GAAGATGCGCGGGAAGTAG-3′; mouse Mdm2-qRT Re, 5′-CATGTTGGTATTGCACATTGG-3′; mouse p53-qRT Fw, 5′-CTAGCATTCAGGCCCTCATC-3′; mouse p53-qRT Re, 5′-TCCGACTGTGACTCCTCCAT-3′; mouse Pak1-qRT Fw, 5′-AACCCAGAGAAGTTGTCAGC-3′; mouse Pak1-qRT Re, 5′-CAATCAGTGGAGTCAGGCTAG-3′; mouse RPL13-qRT Fw, 5′-TGCTGCTCTCAAGGTTGTTCG-3′; mouse RPL13-qRT Re, 5′-GCCTTTTCCTTCCGTTTCTCC-3′.

Statistical analysis

All data, without Fig. 8 H, are expressed as the mean ± SEM of three independent experiments. Comparisons between groups were analyzed with *t* tests.

Online supplemental material

Fig. S1 shows detection of PGAM1 and -2 and validation of the anti-PGAM polyclonal antibody. Fig. S2 shows that Pak1 promotes phosphorylation and

Published February 24, 2014

ubiquitination of PGAM. Fig. S3 shows effects of p53 and Mdm2 on PGAM protein levels. Fig. S4 shows ubiquitination of PGAM2 in vitro and mutation of relevant lysine residues. Fig. S5 shows that Mdm2-M459I affects ubiquitination of both PGAM and p53. Online supplemental material is available at http://www.jcb.org/cgi/content/full/jcb.201306149/DC1.

We thank the staff in the Geriatric Department of Kyoto University for cooperation; Eri Shibata and Setsuo Asahi for providing excellent technical assistance; and Dr. Kayoko Maehara, Dr. Takahiro Matsusaka, Dr. Karen H. Vousden, Dr. Yoshinori Yoshida, and Dr. Jun-ichi Miyazaki for providing experimental materials. The animal experiment and the radio isotope experiment were performed at the institute of Laboratory Animals, Graduate School of Medicine, Kyoto University, and in the Kyoto University Hospital Radioisotopes Research Laboratory, respectively.

T. Maruyama was supported by a postdoctoral fellowship from the Global COE program "Center for Frontier Medicine." This work was supported in part by grants from the Global COE program "Center for Frontier Medicine," from the Japan Society for the Promotion of Science, from the Ministry of Education, Culture, Sports, Science, and Technology of Japan (grants No. 20590696 and No. 23390186), from the Japan Science and Technology Agency (grants No. 8447 and No. 5485), and from Japan Science and Technology Agency (JST) Core Research for Evolutional Science and Technology (CREST No. 18 to H. Kondoh).

The authors declare no competing financial interests.

Submitted: 26 June 2013
Accepted: 10 January 2014

References

Acosta, J.C., A. O'Loghlen, A. Banito, M.V. Guijarro, A. Augert, S. Raguz, M. Fumagalli, M. Da Costa, C. Brown, N. Popov, et al. 2008. Chemokine signaling via the CXCR2 receptor reinforces senescence. *Cell.* 133:1006–1018. http://dx.doi.org/10.1016/j.cell.2008.03.038

Bensaad, K., A. Tsuruta, M.A. Selak, M.N. Vidal, K. Nakano, R. Bartrons, E. Gottlieb, and K.H. Vousden. 2006. TIGAR, a p53-inducible regulator of glycolysis and apoptosis. *Cell.* 126:107–120. http://dx.doi.org/10.1016/j.cell.2006.05.036

Brown, D.R., C.A. Thomas, and S.P. Deb. 1998. The human oncoprotein MDM2 arrests the cell cycle: elimination of its cell-cycle-inhibitory function induces tumorigenesis. *EMBO J.* 17:2513–2525. http://dx.doi.org/10.1093/emboj/17.9.2513

Brummelkamp, T.R., R. Bernards, and R. Agami. 2002. A system for stable expression of short interfering RNAs in mammalian cells. *Science.* 296:550–553. http://dx.doi.org/10.1126/science.1068999

Campisi, J. 2013. Aging, cellular senescence, and cancer. *Annu. Rev. Physiol.* 75:685–705. http://dx.doi.org/10.1146/annurev-physiol-030212-183653

Cancer Genome Atlas Research Network. 2008. Comprehensive genomic characterization defines human glioblastoma genes and core pathways. *Nature.* 455:1061–1068. http://dx.doi.org/10.1038/nature07385

Carnero, A., J.D. Hudson, C.M. Price, and D.H. Beach. 2000. p16INK4A and p19ARF act in overlapping pathways in cellular immortalization. *Nat. Cell Biol.* 2:148–155.

Chen, Q., and B.N. Ames. 1994. Senescence-like growth arrest induced by hydrogen peroxide in human diploid fibroblast F65 cells. *Proc. Natl. Acad. Sci. USA.* 91:4130–4134. http://dx.doi.org/10.1073/pnas.91.10.4130

Dimri, G.P., X. Lee, G. Basile, M. Acosta, G. Scott, C. Roskelley, E.E. Medrano, M. Linskens, I. Rubelj, O. Pereira-Smith, et al. 1995. A biomarker that identifies senescent human cells in culture and in aging skin in vivo. *Proc. Natl. Acad. Sci. USA.* 92:9363–9367. http://dx.doi.org/10.1073/pnas.92.20.9363

Ding, L., G. Getz, D.A. Wheeler, E.R. Mardis, M.D. McLellan, K. Cibulskis, C. Sougnez, H. Greulich, D.M. Muzny, M.B. Morgan, et al. 2008. Somatic mutations affect key pathways in lung adenocarcinoma. *Nature.* 455:1069–1075. http://dx.doi.org/10.1038/nature07423

Durany, N., J. Joseph, E. Campo, R. Molina, and J. Carreras. 1997. Phosphoglycerate mutase, 2,3-bisphosphoglycerate phosphatase and enolase activity and isoenzymes in lung, colon and liver carcinomas. *Br. J. Cancer.* 75:969–977. http://dx.doi.org/10.1038/bjc.1997.168

Durany, N., J. Joseph, O.M. Jimenez, F. Climent, P.L. Fernández, F. Rivera, and J. Carreras. 2000. Phosphoglycerate mutase, 2,3-bisphosphoglycerate phosphatase, creatine kinase and enolase activity and isoenzymes in breast carcinoma. *Br. J. Cancer.* 82:20–27.

Evans, M.J., A. Saghatelian, E.J. Sorensen, and B.F. Cravatt. 2005. Target discovery in small-molecule cell-based screens by in situ proteome reactivity profiling. *Nat. Biotechnol.* 23:1303–1307. http://dx.doi.org/10.1038/nbt1149

Hagai, T., A. Tóth-Petróczy, A. Azia, and Y. Levy. 2012. The origins and evolution of ubiquitination sites. *Mol. Biosyst.* 8:1865–1877. http://dx.doi.org/10.1039/c2mb25052g

Haupt, Y., R. Maya, A. Kazaz, and M. Oren. 1997. Mdm2 promotes the rapid degradation of p53. *Nature.* 387:296–299. http://dx.doi.org/10.1038/387296a0

Hayflick, L. 1965. The limited in vitro lifetime of human diploid cell strains. *Exp. Cell Res.* 37:614–636. http://dx.doi.org/10.1016/0014-4827(65)90211-9

Hershko, A., and A. Ciechanover. 1998. The ubiquitin system. *Annu. Rev. Biochem.* 67:425–479. http://dx.doi.org/10.1146/annurev.biochem.67.1.425

Hitosugi, T., L. Zhou, S. Elf, J. Fan, H.B. Kang, J.H. Seo, C. Shan, Q. Dai, L. Zhang, J. Xie, et al. 2012. Phosphoglycerate mutase 1 coordinates glycolysis and biosynthesis to promote tumor growth. *Cancer Cell.* 22:585–600. http://dx.doi.org/10.1016/j.ccr.2012.09.020

International Cancer Genome Consortium. 2010. International network of cancer genome projects. *Nature.* 464:993–998. (published erratum appears in *Nature.* 2010. 17:465) http://dx.doi.org/10.1038/nature08987

Itahana, K., H. Mao, A. Jin, Y. Itahana, H.V. Clegg, M.S. Lindström, K.P. Bhat, V.L. Godfrey, G.I. Evan, and Y. Zhang. 2007. Targeted inactivation of Mdm2 RING finger E3 ubiquitin ligase activity in the mouse reveals mechanistic insights into p53 regulation. *Cancer Cell.* 12:355–366. http://dx.doi.org/10.1016/j.ccr.2007.09.007

Iyer, N.V., L.E. Kotch, F. Agani, S.W. Leung, E. Laughner, R.H. Wenger, M. Gassmann, J.D. Gearhart, A.M. Lawler, A.Y. Yu, and G.L. Semenza. 1998. Cellular and developmental control of O2 homeostasis by hypoxia-inducible factor 1 alpha. *Genes Dev.* 12:149–162. http://dx.doi.org/10.1101/gad.12.2.149

Jones, R.G., D.R. Plas, S. Kubek, M. Buzzai, J. Mu, Y. Xu, M.J. Birnbaum, and C.B. Thompson. 2005. AMP-activated protein kinase induces a p53-dependent metabolic checkpoint. *Mol. Cell.* 18:283–293. http://dx.doi.org/10.1016/j.molcel.2005.03.027

Kawauchi, K., K. Araki, K. Tobiume, and N. Tanaka. 2008. p53 regulates glucose metabolism through an IKK-NF-κB pathway and inhibits cell transformation. *Nat. Cell Biol.* 10:611–618. http://dx.doi.org/10.1038/ncb1724

Kondoh, H., M.E. Lleonart, J. Gil, J. Wang, P. Degan, G. Peters, D. Martinez, A. Carnero, and D. Beach. 2005. Glycolytic enzymes can modulate cellular life span. *Cancer Res.* 65:177–185.

Koppenol, W.H., P.L. Bounds, and C.V. Dang. 2011. Otto Warburg's contributions to current concepts of cancer metabolism. *Nat. Rev. Cancer.* 11:325–337. http://dx.doi.org/10.1038/nrc3038

Kubbutat, M.H., S.N. Jones, and K.H. Vousden. 1997. Regulation of p53 stability by Mdm2. *Nature.* 387:299–303. http://dx.doi.org/10.1038/387299a0

Kubbutat, M.H., R.L. Ludwig, A.J. Levine, and K.H. Vousden. 1999. Analysis of the degradation function of Mdm2. *Cell Growth Differ.* 10:87–92.

Kuilman, T., C. Michaloglou, L.C. Vredeveld, S. Douma, R. van Doorn, C.J. Desmet, L.A. Aarden, W.J. Mooi, and D.S. Peeper. 2008. Oncogene-induced senescence relayed by an interleukin-dependent inflammatory network. *Cell.* 133:1019–1031. http://dx.doi.org/10.1016/j.cell.2008.03.039

Leach, F.S., T. Tokino, P. Meltzer, M. Burrell, J.D. Oliner, S. Smith, D.E. Hill, D. Sidransky, K.W. Kinzler, and B. Vogelstein. 1993. p53 Mutation and MDM2 amplification in human soft tissue sarcomas. *Cancer Res.* 53:2231–2234.

Li, M., C.L. Brooks, F. Wu-Baer, D. Chen, R. Baer, and W. Gu. 2003. Mono- versus polyubiquitination: differential control of p53 fate by Mdm2. *Science.* 302:1972–1975. http://dx.doi.org/10.1126/science.1091362

Lipkowitz, S., and A.M. Weissman. 2011. RINGs of good and evil: RING finger ubiquitin ligases at the crossroads of tumour suppression and oncogenesis. *Nat. Rev. Cancer.* 11:629–643. http://dx.doi.org/10.1038/nrc3120

Manfredi, J.J. 2010. The Mdm2-p53 relationship evolves: Mdm2 swings both ways as an oncogene and a tumor suppressor. *Genes Dev.* 24:1580–1589. http://dx.doi.org/10.1101/gad.1941710

McClatchey, A.I., I. Saotome, K. Mercer, D. Crowley, J.F. Gusella, R.T. Bronson, and T. Jacks. 1998. Mice heterozygous for a mutation at the Nf2 tumor suppressor locus develop a range of highly metastatic tumors. *Genes Dev.* 12:1121–1133. http://dx.doi.org/10.1101/gad.12.8.1121

Molli, P.R., D.Q. Li, B.W. Murray, S.K. Rayala, and R. Kumar. 2009. PAK signaling in oncogenesis. *Oncogene.* 28:2545–2555. http://dx.doi.org/10.1038/onc.2009.119

Niwa, H., K. Yamamura, and J. Miyazaki. 1991. Efficient selection for high-expression transfectants with a novel eukaryotic vector. *Gene.* 108:193–199. http://dx.doi.org/10.1016/0378-1119(91)90434-D

Ogawara, Y., S. Kishishita, T. Obata, Y. Isazawa, T. Suzuki, K. Tanaka, N. Masuyama, and Y. Gotoh. 2002. Akt enhances Mdm2-mediated ubiquitination and degradation of p53. *J. Biol. Chem.* 277:21843–21850. http://dx.doi.org/10.1074/jbc.M109745200

Published February 24, 2014

Osthus, R.C., H. Shim, S. Kim, Q. Li, R. Reddy, M. Mukherjee, Y. Xu, D. Wonsey, L.A. Lee, and C.V. Dang. 2000. Deregulation of glucose transporter 1 and glycolytic gene expression by c-Myc. *J. Biol. Chem.* 275:21797–21800. http://dx.doi.org/10.1074/jbc.C000023200

Parrinello, S., E. Samper, A. Krtolica, J. Goldstein, S. Melov, and J. Campisi. 2003. Oxygen sensitivity severely limits the replicative lifespan of murine fibroblasts. *Nat. Cell Biol.* 5:741–747. http://dx.doi.org/10.1038/ncb1024

Poyurovsky, M.V., X. Jacq, C. Ma, O. Karni-Schmidt, P.J. Parker, M. Chalfie, J.L. Manley, and C. Prives. 2003. Nucleotide binding by the Mdm2 RING domain facilitates Arf-independent Mdm2 nucleolar localization. *Mol. Cell.* 12:875–887. http://dx.doi.org/10.1016/S1097-2765(03)00400-3

Prives, C. 1998. Signaling to p53: breaking the MDM2-p53 circuit. *Cell.* 95:5–8. http://dx.doi.org/10.1016/S0092-8674(00)81774-2

Reifenberger, G., L. Liu, K. Ichimura, E.E. Schmidt, and V.P. Collins. 1993. Amplification and overexpression of the MDM2 gene in a subset of human malignant gliomas without p53 mutations. *Cancer Res.* 53:2736–2739.

Ren, F., H. Wu, Y. Lei, H. Zhang, R. Liu, Y. Zhao, X. Chen, D. Zeng, A. Tong, L. Chen, et al. 2010. Quantitative proteomics identification of phosphoglycerate mutase 1 as a novel therapeutic target in hepatocellular carcinoma. *Mol. Cancer.* 9:81. http://dx.doi.org/10.1186/1476-4598-9-81

Rodrigues, N.R., A. Rowan, M.E. Smith, I.B. Kerr, W.F. Bodmer, J.V. Gannon, and D.P. Lane. 1990. p53 mutations in colorectal cancer. *Proc. Natl. Acad. Sci. USA.* 87:7555–7559. http://dx.doi.org/10.1073/pnas.87.19.7555

Ruiz-Lozano, P., M.L. Hixon, M.W. Wagner, A.I. Flores, S. Ikawa, A.S. Baldwin Jr., K.R. Chien, and A. Gualberto. 1999. p53 is a transcriptional activator of the muscle-specific phosphoglycerate mutase gene and contributes in vivo to the control of its cardiac expression. *Cell Growth Differ.* 10:295–306.

Samuels-Lev, Y., D.J. O'Connor, D. Bergamaschi, G. Trigiante, J.K. Hsieh, S. Zhong, I. Campargue, L. Naumovski, T. Crook, and X. Lu. 2001. ASPP proteins specifically stimulate the apoptotic function of p53. *Mol. Cell.* 8:781–794. http://dx.doi.org/10.1016/S1097-2765(01)00367-7

Schraml, P., G. Schwerdtfeger, F. Burkhalter, A. Raggi, D. Schmidt, T. Ruffalo, W. King, K. Wilber, M.J. Mihatsch, and H. Moch. 2003. Combined array comparative genomic hybridization and tissue microarray analysis suggest PAK1 at 11q13.5-q14 as a critical oncogene target in ovarian carcinoma. *Am. J. Pathol.* 163:985–992. http://dx.doi.org/10.1016/S0002-9440(10)63458-X

Seger, Y.R., M. García-Cao, S. Piccinin, C.L. Cunsolo, C. Doglioni, M.A. Blasco, G.J. Hannon, and R. Maestro. 2002. Transformation of normal human cells in the absence of telomerase activation. *Cancer Cell.* 2:401–413. http://dx.doi.org/10.1016/S1535-6108(02)00183-6

Serrano, M., H. Lee, L. Chin, C. Cordon-Cardo, D. Beach, and R.A. DePinho. 1996. Role of the INK4a locus in tumor suppression and cell mortality. *Cell.* 85:27–37. http://dx.doi.org/10.1016/S0092-8674(00)81079-X

Serrano, M., A.W. Lin, M.E. McCurrach, D. Beach, and S.W. Lowe. 1997. Oncogenic ras provokes premature cell senescence associated with accumulation of p53 and p16INK4a. *Cell.* 88:593–602. http://dx.doi.org/10.1016/S0092-8674(00)81902-9

Shalom-Barak, T., and U.G. Knaus. 2002. A p21-activated kinase-controlled metabolic switch up-regulates phagocyte NADPH oxidase. *J. Biol. Chem.* 277:40659–40665. http://dx.doi.org/10.1074/jbc.M206650200

Terzian, T., Y.A. Suh, T. Iwakuma, S.M. Post, M. Neumann, G.A. Lang, C.S. Van Pelt, and G. Lozano. 2008. The inherent instability of mutant p53 is alleviated by Mdm2 or p16INK4a loss. *Genes Dev.* 22:1337–1344. http://dx.doi.org/10.1101/gad.1662908

Thorslund, T., F. Esashi, and S.C. West. 2007. Interactions between human BRCA2 protein and the meiosis-specific recombinase DMC1. *EMBO J.* 26:2915–2922. http://dx.doi.org/10.1038/sj.emboj.7601739

Vadlamudi, R.K., L. Adam, R.A. Wang, M. Mandal, D. Nguyen, A. Sahin, J. Chernoff, M.C. Hung, and R. Kumar. 2000. Regulatable expression of p21-activated kinase-1 promotes anchorage-independent growth and abnormal organization of mitotic spindles in human epithelial breast cancer cells. *J. Biol. Chem.* 275:36238–36244. http://dx.doi.org/10.1074/jbc.M002138200

Vander Heiden, M.G., L.C. Cantley, and C.B. Thompson. 2009. Understanding the Warburg effect: the metabolic requirements of cell proliferation. *Science.* 324:1029–1033. http://dx.doi.org/10.1126/science.1160809

Vander Heiden, M.G., J.W. Locasale, K.D. Swanson, H. Sharfi, G.J. Heffron, D. Amador-Noguez, H.R. Christofk, G. Wagner, J.D. Rabinowitz, J.M. Asara, and L.C. Cantley. 2010. Evidence for an alternative glycolytic pathway in rapidly proliferating cells. *Science.* 329:1492–1499. http://dx.doi.org/10.1126/science.1188015

Wang, R.A., A. Mazumdar, R.K. Vadlamudi, and R. Kumar. 2002. P21-activated kinase-1 phosphorylates and transactivates estrogen receptor-α and promotes hyperplasia in mammary epithelium. *EMBO J.* 21:5437–5447. http://dx.doi.org/10.1093/emboj/cdf543

Warburg, O. 1956. On respiratory impairment in cancer cells. *Science.* 124:269–270.

Zhang, S., J. Han, M.A. Sells, J. Chernoff, U.G. Knaus, R.J. Ulevitch, and G.M. Bokoch. 1995. Rho family GTPases regulate p38 mitogen-activated protein kinase through the downstream mediator Pak1. *J. Biol. Chem.* 270:23934–23936. http://dx.doi.org/10.1074/jbc.270.41.23934

Zhang, J., L. Yu, Q. Fu, J. Gao, Y. Xie, J. Chen, P. Zhang, Q. Liu, and S. Zhao. 2001. Mouse phosphoglycerate mutase M and B isozymes: cDNA cloning, enzyme activity assay and mapping. *Gene.* 264:273–279. http://dx.doi.org/10.1016/S0378-1119(00)00597-7

Zwerschke, W., S. Mazurek, P. Stöckl, E. Hütter, E. Eigenbrodt, and P. Jansen-Dürr. 2003. Metabolic analysis of senescent human fibroblasts reveals a role for AMP in cellular senescence. *Biochem. J.* 376:403–411. http://dx.doi.org/10.1042/BJ20030816

Ann Surg Oncol (2013) 20:2213–2218
DOI 10.1245/s10434-013-2890-0

Annals of
SURGICAL ONCOLOGY
OFFICIAL JOURNAL OF THE SOCIETY OF SURGICAL ONCOLOGY

ORIGINAL ARTICLE – BREAST ONCOLOGY

Comparison of the Indocyanine Green Fluorescence and Blue Dye Methods in Detection of Sentinel Lymph Nodes in Early-stage Breast Cancer

Tomoharu Sugie, MD[1], Terumasa Sawada, MD[2], Nobumi Tagaya, MD[3], Takayuki KinoshitaMD[4], Kazuhiko Yamagami, MD[5], Hirofumi SuwaMD[6], Takafumi Ikeda, PhD[7], Kenichi Yoshimura, PhD[7], Miyuki Niimi, PhD[7], Akira Shimizu, MD[7], and Masakazu Toi, MD[1]

[1]Department of Breast Surgery, Kyoto University, Kyoto, Japan; [2]Department of Breast Surgical Oncology, Showa University, Tokyo, Japan; [3]Department of Surgery, Dokkyo Medical University, Koshigaya Hospital, Koshigaya, Japan; [4]Department of Breast Surgery, National Cancer Center Hospital, Tokyo, Japan; [5]Department of Breast Surgery, Shinko Hospital, Kobe, Japan; [6]Department of Breast Surgery, Hyogo Prefectural Tsukaguchi Hospital, Amagasaki, Japan; [7]Translation Research Center, Kyoto University Hospital, Kyoto, Japan

ABSTRACT

Purpose. To assess the diagnostic performance of sentinel lymph node (SLN) biopsy using the indocyanine green (ICG) fluorescence method compared with that using the blue dye method, a prospective multicenter study was performed.

Methods. Patients with T1–3 primary breast cancer without clinical lymph node involvement were included in this study. ICG as a fluorescence-emitting source and indigo carmine as blue dye were injected into the subareolar area. Extracted lymph nodes were examined to identify the first, second, and other SLNs. The identified nodes were classified according to the ICG fluorescence signal and blue dye uptake.

Results. Ninety-nine eligible patients were included in this study. The ICG fluorescence method identified an average of 3.4 SLNs (range, 1–8) in 98 of 99 patients (detection rate, 99 %). The number of lymph nodes identified by the fluorescence method was significantly higher than that identified by the blue dye method ($p < 0.001$). SLN involvement was identified in 20 % (20 of 99) of patients, all of whom tested positive for the first SLN. In 16 patients, complete axillary lymph node dissection (ALND) was performed. In 25 % (4 of 16) of these patients, axillary metastases were identified; however, no axillary involvement was found in 8 patients with only one involved node, which was isolated as the first SLN.

Conclusions. High rate of SLN detection was achieved using the ICG fluorescence method. The first SLN identified by fluorescence imaging provides an exact indication of the axillary status. Therefore, the ICG fluorescence method provides precise information required to avoid unnecessary ALND.

For many years, axillary lymph node dissection (ALND) has been performed for prevention of lymph node metastasis in patients with breast cancer. However, ALND is associated with a relatively high risk of complications such as edema of the arms (lymphedema), dyskinesia, and pain, which lower quality of life.[1–3] In the 1990s, sentinel lymph node (SLN) biopsy was proposed for the assessment of axillary lymph node involvement to circumvent unnecessary ALND.

Sentinel lymph node is defined as a lymph node that receives lymph flow directly from the primary tumor. Because this concept was first applied to melanoma patients in 1992, SLN biopsy has become a standard method for evaluating the axillary lymph node status in patients with early-stage breast cancer.[4–7] The following two methods are commonly utilized for detecting SLNs: the radioimmunoassay (RI) method, which involves application of radioactive colloids, and injection of blue dye.[8,9] Both methods have their advantages and

First Received: 31 July 2012;
Published Online: 21 February 2013

T. Sugie, MD
e-mail: sugie@kuhp.kyoto-u.ac.jp

disadvantages.[10–12] The RI method has the advantage of a high SLN identification rate, while disadvantages include the requirement of a radioactive facility, exposure to radiation, and high cost. In contrast, the blue dye method has the advantages of a high prevalence rate, no radiation exposure, and low cost; however, SLN identification rates are lower with this method compared with the RI method.[13] Furthermore, the success of the blue dye method is dependent on the technician's skill and experience.[14]

Indocyanine green (ICG) is a dye on which laser-emitting diodes are centered at 760 nm to collect fluorescence at 830 nm. The fluorescing property of the ICG reagent was first applied to the dye method, followed by the fluorescence method.[15] The ICG fluorescence method requires a photodynamic eye (PDE) camera. It lacks the stringent safety controls of the RI method. Therefore, the fluorescence method is not limited to use in high-volume centers. Lymph flow can be confirmed as a real-time image from outside the body using the ICG fluorescence method; therefore, this method is well suited for performing intraoperative SLN biopsy.

Because the ICG fluorescence method requires little skill and the necessary reagents and apparatus are inexpensive in comparison with the RI method, use of the former method at the physician's discretion has been increasing. Recent clinical results obtained after introduction of the ICG fluorescence method have indicated higher SLN identification rates than those observed with the blue dye method.[16–19] However, operational procedures and experience of the personnel vary among institutions. In addition, no statistical analysis has clearly demonstrated the superiority of the ICG fluorescence method over the blue dye method. The present multicenter, cooperative, prospective analysis using a standardized procedure was performed to demonstrate the efficacy of the ICG fluorescence method in comparison with that of the blue dye method.

METHODS

Patients

Eligible patients were 20–75 years old at registration and diagnosed with T1–3 primary breast cancer without clinical lymph node metastasis (N0). Six participating centers in Japan have been governmentally authorized to perform SLN biopsy. SLN biopsies were performed by ten well-trained physicians according to a standard written procedure. This study was performed in accordance with the Declaration of Helsinki, and all patients provided written informed consent. The study protocol was approved by the local ethics committees at all participating trial sites. Patients in whom previous surgical biopsy or surgery involving the axillary regions had been performed, those in whom preoperative drug therapy (including hormone therapy and chemotherapy) had been administered, and those who had a history of allergy to ICG or indigo carmine dye were excluded from the study.

Surgical Procedure

All surgeons performed SLN biopsy following the standard procedure. In this study, SLNs were categorized as follows: axillary lymph nodes, blue-stained (true SLN); axillary lymph nodes, ICG fluorescence-positive detected by PDE (true SLN); and palpably suspicious, surgically removed lymph nodes in which neither ICG fluorescence nor blue dye was found (para-SLN). The surgeon's goal during the procedure was to remove the blue-stained and/or fluorescent lymph nodes (true SLNs) in the incised region. Palpated lymph nodes in the operative area were also removed as para-SLN.

The ICG fluorescence method has been previously reported.[17] In brief, 0.5–1 ml of 0.5 % ICG as a source of fluorescence and 2–4 ml of indigo carmine as a blue dye were injected in the subareolar area. Lymphatic flow was then traced with a PDE camera (a charge-coupled device; Hamamatsu Photonics Co., Hamamatsu, Japan). Real-time, image-guided surgery was used to identify the fluorescence signals of the SLNs after meticulous dissection. The excised lymph nodes were examined separately according to the order of removal and classified according to detection by ICG fluorescence and/or blue dye.

Study Objectives

The primary endpoint in this study was to determine the number of lymph nodes identified by each method. In each patient, all extracted lymph nodes were classified into four categories on the basis of the two detection methods as follows: SLNs identified by both fluorescence and blue dye (flu^+/dye^+), those identified by fluorescence only (flu^+/dye^-), those identified by dye only (flu^-/dye^+), and those in which neither fluorescence nor dye was observed (para-SLNs; flu^-/dye^-). Secondary endpoints included the SLN identification rate, SLN metastasis rate, and metastasis rate according to the order of SLN detection.

Statistical Methods

The number of lymph nodes identified using the ICG fluorescence method and that using the blue dye method were compared. Differences were calculated by subtracting the number of flu^-/dye^+ SLNs from the number of flu^+/dye^- SLNs for each patient. The sign test was used to test the null hypothesis that the number of identified lymph

nodes was equal. The identification rate via fluorescence or blue dye was defined by the proportion of patients with SLNs identified with either method. Exact 95 % confidence intervals were obtained on the basis of binomial distribution. Subgroup analyses of the SLN identification rate were conducted according to age and body mass index (BMI) using Fisher's exact test. Metastasis rates were separately obtained for flu^+/dye^+ SLNs, flu^+/dye^- SLNs, flu^-/dye^+ SLNs, and para-SLNs (flu^-/dye^-). They were also separately obtained for ordered flu^+ SLNs. The prevalence of adverse events was assessed. In order to use the sign test (alpha, 0.05; power, 0.90), results from 100 patients were required to detect whether the number of flu^+/dye^- SLNs was greater than that of flu^-/dye^+ SLNs in 66 % or more of eligible patients.

RESULTS

From February to October 2010, SLN biopsy was performed in 100 patients (mean age, 60 years; range, 29–75 years) with early-stage breast cancer. One patient was excluded in whom hormone therapy was administered before biopsy. Thus, 99 patients were eligible for further assessment. Of these, ductal carcinoma in situ was diagnosed in 7 %, while invasive ductal carcinoma was diagnosed in 93 %. Patient and tumor characteristics are summarized in Table 1.

Overall, the ICG fluorescence method identified an average of 3.4 SLNs in 98 of 99 patients (detection rate, 99 %). The median difference between the number of lymph nodes identified by the fluorescence and blue dye methods was one (range, 0–6 nodes), and the number of SLNs identified by the former method was significantly higher than that identified by the latter method ($p < 0.001$). Therefore, the SLN detection rate using the ICG fluorescence method was significantly higher than that by the dye method (99 vs. 78 %, $p < 0.001$; Table 2). Furthermore, SLN identification by fluorescence was independent of age and BMI (Table 3).

Table 4 summarizes the data obtained from the 99 patients ($n = 340$ SLN specimens) by the detection method. Of these patients, positive SLN identification was achieved by both methods in 78 % (77 of 99, flu^+/dye^+), ICG fluorescence alone detected SLNs in 69 % (68 of 99, flu^+/dye^-), and para-SLNs were identified in 35 % (35 of 99, flu^-/dye^-). In these 35 patients, true SLNs were identified using the ICG fluorescence and/or blue dye methods; in no patient were para-SLNs found alone. No SLNs were classified as flu^-/dye^+. Of the 340 specimens, true SLNs categorized as flu^+/dye^+ and flu^+/dye^- accounted for 36 % (121 of 340) and 47 % (160 of 340), respectively. Though para-SLNs (flu^-/dye^-) were identified in 17 % (59 of 340)

TABLE 1 Patients and tumor characteristics ($n = 99$)

Characteristic	Value
Age, years, mean (range)	60 (29–75)
Pathology	
Invasive ductal carcinoma	92 (93 %)
Noninvasive ductal carcinoma	7 (7 %)
Clinical tumor size	
Tis	4 (4 %)
T1a	4 (4 %)
T1b	15 (15 %)
T1c	39 (39 %)
T2	34 (34 %)
T3	1 (1 %)
Tx	2 (2 %)
Grade	
1	36 (36 %)
2	37 (37 %)
3	23 (23 %)
Unknown	3 (3 %)
Estrogen receptor	
Negative	17 (17 %)
Positive	81 (82 %)
Unknown	1 (1 %)
Progesterone receptor	
Negative	24 (24 %)
Positive	73 (74 %)
Unknown	2 (2 %)
HER2	
Negative	37 (37 %)
1+	32 (32 %)
2+	15 (15 %)
3+	12 (12 %)
Unknown	3 (3 %)
BMI (kg/m^2)	
<18.5	11 (11 %)
≥18.5, <22	39 (39 %)
≥22, <25	32 (32 %)
≥25 <30	13 (13 %)
≥30	4 (4 %)

BMI body mass index

TABLE 2 Comparison of sentinel lymph node detection between the ICG fluorescence method and the dye method

Characteristic	Result	*p*
Difference in number of lymph nodes identified		
Difference (ICG fluorescence–blue dye)	1.0 (range, 0–6)	<0.001
Detection rate		
ICG fluorescence	99 % (98/99)	<0.001
Dye	78 % (77/99)	

ICG indocyanine green

TABLE 3 SLN detection rate according to age and BMI using the ICG fluorescence method and the dye method

Characteristic	ICG (%)	p^a	Dye (%)	p^a
Age (years)				
<50	100 (30/30)	1.00	87 (26/30)	0.03
≥50, <60	100 (19/19)		95 (18/19)	
≥60, <70	97 (34/35)		69 (24/35)	
≥70	100 (15/15)		60 (9/15)	
BMI (kg/m^2)				
<18.5	100 (11/11)	0.61	100 (11/11)	0.20
≥18.5, <22	100 (39/39)		79 (31/39)	
≥22, <25	97 (31/32)		75 (24/32)	
≥25, <30	100 (13/13)		62 (8/13)	
≥30	100 (4/4)		75 (3/4)	

SLN sentinel lymph node, *BMI* body mass index, *ICG* indocyanine green

[a] Fisher's exact test

TABLE 4 Classification of SLN in terms of fluorescence and dye

Characteristic	Patients, % (n = 99)	SLNs identified, % (n = 340)
Flu$^+$/dye$^+$	78 (77/99)	36 (121/340)
Flu$^+$/dye$^-$	69 (68/99)	47 (160/340)
Flu$^-$/dye$^+$	0 (0/99)	0 (0/340)
Flu$^-$/dye$^-$	35 (35/99)	17 (59/340)

SLN sentinel lymph node, *flu* fluorescence

of these specimens, 100 % of the lymph nodes were ICG fluorescence-positive if para-SLNs were excluded.

Table 5 summarizes SLN and non-SLN involvement in order of SLN removal. The first SLN was defined as the proximal lymph node draining lymphatic flow from the tumor. Involvement of the first SLN was exhibited in all 20 % (20 of 99) of the patients with positive lymph nodes. Of these 20, the first isolated node was the only positive node in 12 (60 %; 9 flu$^+$/dye$^+$, 3 flu$^+$/dye$^-$). Metastases in the second or further SLNs were identified in eight patients, all of whom had a positive first SLN. In 16 of the 20 SLN-positive patients, complete ALND was performed. No axillary lymph node involvement was detected in all eight patients with the first SLN as the only positive lymph node, whereas non-SLN metastases were not detected in 4 of 8 (50 %) patients with positive second or further lymph nodes in addition to the first positive SLN. No skin necrosis or tattoo relevant to subcutaneous ICG injection was observed. No shock or other adverse reactions due to hypersensitivity were noted.

TABLE 5 SLN and non-SLN involvement in terms of the order of SLN removal

Characteristic	Patients, %
Patients with positive SLNs	20 (20/99)
Positive SLN identified by:	
ICG	100 (20/20)
Dye	70 (14/20)
First SLN positive alone	60 (12/20)
Completion of ALND	67 (8/12)
Non-SLN negative	100 (8/8)
Non-SLN positive	0 (0/8)
First SLN and second or further positive	40 (8/20)
Completion of ALND	100 (8/8)
Non-SLN negative	50 (4/8)
Non-SLN positive	50 (4/8)

SLN sentinel lymph node, *ICG* indocyanine green

DISCUSSION

This is the first prospective study to evaluate the efficacy of SLN detection using the ICG fluorescence method. The detection rate using this method was significantly higher than that using the indigo carmine or blue dye method in patients with early breast cancer. This high detection rate may be a consequence of the greater optical sensitivity of ICG compared to the color perception of the blue dye. In previous studies, the use of ICG without fluorescence imaging did not improve the SLN detection rate (73.8 %), whereas the ICG fluorescence method used in our study achieved a detection rate of 99 %, which was comparable to that reported in previous studies.[15–20]

The ICG fluorescence method uses an integrated dye coupled with an infrared camera equipped with a 765-nm wavelength emitter. Emitted near-infrared radiation activates ICG molecules and fluorescence emissions at a wavelength of 830 nm. This makes lymphatic flow and drainage of SLNs visible as fluorescence signals. Fluorescence imaging assists the surgeon in navigating the axillary basin along the subcutaneous vessels and enables orderly and sequential SLN dissection.

Obesity is associated with the development and recurrence of breast cancer.[21,22] Obesity may inhibit accurate identification of SLNs.[23,24] As the emitted fluorescence is more attenuated through fat droplets, fluorescence may decrease in proportion to increased body mass. In preliminary studies, detection of fluorescence signals deeper than 1 cm from the skin level was difficult. Abe et al.[25] reported a significant correlation between BMI and the time and depth required to reach SLNs in the axilla. In the current study, a stable SLN detection rate was observed using ICG fluorescence regardless of BMI, whereas the

detection rate using indigo carmine dye tended to decrease as BMI increased (NS). Thus, detection of SLN by ICG fluorescence is stable regardless of BMI, which may or may not reduce operative time compared to blue dye alone. The median BMI in patients included in the present study was 21.8 kg/m^2 (range, 17.6–32.4 kg/m^2). Only 4 % of patients had a BMI > 30 kg/m^2. As obesity is more prevalent in Caucasians than in Asians, the relationship between BMI and accuracy of SLN detection using ICG fluorescence requires further investigation in the former population. Skin compression techniques have been recently developed to ameliorate the attenuation of fluorescence signals. Skin compression is a simple procedure to overcome the weaknesses of the fluorescence technique in obese patients.[26]

Because lymph flow alters with age, older age may be significantly associated with false-negative SLN biopsy results. Cox et al.[23] reported that RI counts in SLNs were inversely correlated with age. In this study, the SLN detection rate using indigo carmine dye also decreased significantly with age, while the ICG fluorescence method achieved a stable and high detection rate, even in older patients.

In this study, fluorescence-positive and dye-positive (i.e., double positive) SLNs were detected in most patients (78 %). Using the ICG fluorescence method, the first SLN can be identified as the lymph node proximal to the tumor on the basis of drainage patterns and lymphatic flow. By contrast, with the RI method, identifying SLNs in order is difficult because they are detected as hot spots regardless of the anatomical lymphatic flow. In this study, all patients with SLN involvement had positive first SLNs. This means that the first SLN detected by ICG fluorescence imaging represents the exact axillary status.

The number of SLNs resected using fluorescence imaging tends to be higher than that resected using the RI method. In this study, the median number of resected SLNs was 3.4, which was greater than that (1.7–2) reported in studies using the RI method.[5–7] This disadvantage was because of the higher optical sensitivity of fluorescence imaging and the low molecular weight of ICG, which can spread further within the lymphatic basin than blue dye. However, a positive SLN is usually identified within the first 4 resected SLNs.[27] Removal of $\leq$4 nodes is acceptable for optimal accuracy of SLN biopsy.[28,29]

The avoidance of routine application of ALND in patients with positive SLNs is currently under debate in terms of breast cancer outcome. If the tumor burden on SLNs is low, locoregional recurrence can be controlled by irradiation, adjuvant chemotherapy, and hormonal therapy. The Austrian Breast and Colorectal Cancer Study Group (ABCSG Z0011) study reported outcomes of $\leq$2 SLN-positive patients in both ALND and non-ALND cohorts.[30] If axillary clearance was omitted in patients who met the ABCSG Z0011 criteria, three or more SLNs could be resected, which is compatible with the ICG fluorescence method.

In this study, ALND procedures were unnecessarily performed in 75 % (12 of 16) of the patients with positive SLNs, whereas residual axillary disease was found in the remaining 25 % (4 of 16). Of the eight patients with a positive lymph node isolated as the first SLN, none had residual axillary disease. These results suggested that SLN biopsy can safely replace axillary clearance for surgeons otherwise willing to perform further axillary treatment. However, a direct comparison between the ICG fluorescence method and the RI method is required for ensuring the efficacy of the former method. A small study ($n = 30$) has already reported a high SLN detection rate using the ICG fluorescence method. Use of this method decreased the false-negative rate associated with the RI method when both methods were combined.[31] A study using three tracer agents (RI, blue dye, and ICG) recently confirmed the combination of ICG and blue dye method had the highest nodal sensitivity, which avoids the need for radioisotopes.[32] A large-scale prospective study is currently ongoing to test the concordance between these methods. This study may lead to a new proposal for the optimal method of SLN detection and subsequent axillary management in patients with early-stage breast cancer.

ACKNOWLEDGMENT We are grateful to the medical staff of the Translational Research Center, Kyoto University, for their valuable help and scientific advice.

REFERENCES

1. Schrenk P, Rieger R, Shamiyeh A, et al. Morbidity following sentinel lymph node biopsy versus axillary lymph node dissection for patients with breast carcinoma. *Cancer.* 2000;88:608–14.
2. Giuliano AE, Haigh PI, Brennan MB, et al. Prospective observational study of sentinel lymphadenectomy without further axillary dissection in patients with sentinel node-negative breast cancer. *J Clin Oncol.* 2000;18:2553–9.
3. Purushotham AD, Upponi S, Klevesath MB, et al. Morbidity after sentinel lymph node biopsy in primary breast cancer: results from a randomized controlled trial. *J Clin Oncol.* 2005;23:4312–21.
4. Morton DL, Wen DR, Wong JH, et al. Technical details of intraoperative lymphatic mapping for early stage melanoma. *Arch Surg.* 1992;127:392–9.
5. Veronesi U, Paganelli G, Viale G, et al. A randomized comparison of sentinel-node biopsy with routine axillary dissection in breast cancer. *N Engl J Med.* 2003;349:546–53.
6. Krag DN, Anderson SJ, Julian TB, et al. Sentinel-lymph-node resection compared with conventional axillary-lymph-node dissection in clinically node-negative patients with breast cancer: overall survival findings from the NSABP B-32 randomized phase 3 trial. *Lancet Oncol.* 2010;11:927–33.
7. Mansel RE, Fallowfield L, Kissin M, et al. Randomized multicenter trial of sentinel node biopsy versus standard axillary treatment in operable breast cancer: the ALMANAC trial. *J Natl Cancer Inst.* 2006;98:599–609.

8. Krag DN, Weaver DL, Alex JC, et al. Surgical resection and radio-localization of the sentinel node in breast cancer using a gamma probe. *Surg Oncol.* 1993;2:335–40.
9. Giuliano AE, Kirgan DM, Guenther JM, et al. Lymphatic mapping and sentinel lymphadenectomy for breast cancer. *Ann Surg.* 1994;220:391–401.
10. McMasters KM, Tuttle TM, Carlson DJ, et al. Sentinel lymph node biopsy for breast cancer: a suitable alternative to routine axillary dissection in multi-institutional practice when optimal technique in used. *J Clin Oncol.* 2000;18:2560–6.
11. Cody HS 3rd, Fey J, Akhurst T, et al. Complementarity of blue dye and isotope in sentinel node localization for breast cancer: univariate and multivariate analysis of 966 procedures. *Ann Surg Oncol.* 2001;18:2560–6.
12. Tafra L, Lannin DR, Swanson MS, et al. Multicenter trial of sentinel node biopsy for breast cancer using both technetium sulfur colloid and isosulfan blue dye. *Ann Surg.* 2001;233:51–9.
13. Kin T, Guiliano AE, Lyman GH. Lymphatic mapping and sentinel lymph node biopsy in early-stage breast carcinoma. *Cancer.* 2006;106:4–16.
14. Morrow M, Rademaker AW, Bethke KP, et al. Learning sentinel node biopsy: results of a prospective randomized trial of two techniques. *Surgery.* 1999;126:714–20.
15. Kitai T, Inomoto T, Miwa M, Shikayama T. Fluorescence navigation with indocyanine green for detecting sentinel lymph nodes in breast cancer. *Breast Cancer.* 2005;12:211–5.
16. Tagaya N, Yamazaki R, Nakagawa A, et al. Intraoperative identification of sentinel lymph nodes by near-infrared fluorescence imaging inpatients with breast cancer. *Am J Surg.* 2008; 195:850–3.
17. Sugie T, Kassim KA, Takeuchi M, et al. A novel method for sentinel lymph node biopsy by indocyanine green fluorescence technique in breast cancer. *Cancers.* 2010;2:713–20.
18. Hojo T, Nagao T, Kikuyama M, et al. Evaluation of sentinel node biopsy by combined fluorescent and dye method and lymph flow for breast cancer. *Breast.* 2010;19:210–3.
19. Hishch C, Murawa D, Mohr Z, et al. ICG fluorescence-guided sentinel node biopsy for axillary nodal staging in breast cancer. *Breast Cancer Res Treat.* 2010;121:373–8.
20. Motomura K, Inaji H, Komoike Y, et al. Sentinel node biopsy guided by indocyanine green dye in breast cancer patients. *Jpn J Clin Oncol.* 1999;29:604–7.
21. Anderson GL, Neuhouser ML. Obesity and the risk for premenopausal and postmenopausal breast cancer. *Cancer Prev Res (Phila).* 2012;5:515–21.
22. Healy LA, Ryan AM, Rowley S, et al. Obesity increases the risk of postmenopausal breast cancer and is associated with more advanced stage at presentation but no impact on survival. *Breast J.* 2010;16:95–7.
23. Cox CE, Dupont E, Whitehead GF, et al. Age and body mass index may increase the chance of failure in sentinel lymph node biopsy for women with breast cancer. *Breast J.* 2002;8:88–91.
24. Hughes M, Goffman TG, Perry RR, et al. Obesity and lymphatic mapping with sentinel lymph node biopsy in breast cancer. *Am J Surg.* 2004;187:52–7.
25. Abe H, Umeda T, Mori M, et al. Indocyanine green fluorescence imaging system for sentinel lymph node biopsy in early breast cancer patients. *J Clin Oncol.* 2010;28(Suppl. 15):6492.
26. Kitai T, Kawashima M. Transcutaneous detection and direct approach to the sentinel node using axillary compression technique in ICG fluorescence-navigated sentinel node biopsy for breast cancer. *Breast Cancer.* 2012;19:343–8.
27. Zakaria S, Degnim AC, Kleer CG, et al. Sentinel lymph node biopsy for breast cancer: how many nodes are enough? *J Surg Oncol.* 2007;96:554–9.
28. Toi M, Winer EP, Inamoto T, et al. Identifying gaps in the locoregional management of early breast cancer: highlights from the Kyoto Consensus Conference. *Ann Surg Oncol.* 2011;18: 2885–92.
29. Ban EJ, Lee JS, Koo JS, et al. How many sentinel lymph nodes are enough for accurate axillary staging in t1–2 breast cancer? *J Breast Cancer.* 2011;14:296–300.
30. Giuliano AE, Hunt KK, Ballman KV, et al. Axillary dissection vs no axillary dissection in women with invasive breast cancer and sentinel node metastasis: a randomized clinical trial. *JAMA.* 2011;305:569–75.
31. Murawa D, Hirche C, Dresel S, et al. Sentinel lymph node biopsy in breast cancer guided by indocyanine green fluorescence. *Br J Surg.* 2009;96:1289–94.
32. Wishart GC, Loh SW, Jones L, et al. A feasibility study (ICG-10) of indocyanine green (ICG) fluorescence mapping for sentinel lymph node detection in early breast cancer. *Eur J Surg Oncol.* 2012;38:651–6.

Journal of
Clinical Pharmacy and Therapeutics

Journal of Clinical Pharmacy and Therapeutics, 2013, **38**, 309–313 doi: 10.1111/jcpt.12064

Analysis of new drugs whose clinical development and regulatory approval were hampered during their introduction in Japan

R. Asada*† MSc, S. Shimizu‡ PhD, S. Ono§ PhD, T. Ito* PhD, A. Shimizu* PhD and T. Yamaguchi† PhD

**Department of Experimental Therapeutics Translational Research Center, Kyoto University Hospital, Kyoto, †Department of Biostatistics, Tohoku University Graduate School of Medicine, Sendai, ‡Center for Advanced Medicine and Clinical Research, Nagoya University Hospital, Nagoya, and §Laboratory of Pharmaceutical Regulatory Science, Graduate School of Pharmaceutical Sciences, University of Tokyo, Tokyo, Japan*

Received 2 October 2012, Accepted 12 March 2013

Keywords: **clinical data package, clinical trial designs, drug development failures, new drug applications**

SUMMARY

What is known and Objective: **Many drugs fail during development. However, detailed reasons for failure during drug development are almost never disclosed. We focused on the drugs whose clinical development and registration were initially hampered, but which were finally approved to identify reasons that delayed their marketing approval in Japan.**

Methods: **We analysed 727 new drug applications (NDAs) approved in Japan between 2001 and 2011.**

Results and Discussion: **Fifty-three NDAs had serious and identifiable problems during drug development. Of these, 43 NDAs had 'problem related to clinical data'. We found that the problems for withdrawal of these NDAs could be ascribed largely to inappropriate clinical data package and study design for supporting the intended indications and usage and to unclear clinical results for defining dosage regimen or efficacy of the drugs.**

What is new and Conclusion: **Our results indicate the importance of careful determination of the optimal dosage regimen and the choice of objective endpoints in clinical trials. Further, it is important to establish a clear strategy for generating the clinical data package, to include careful design of clinical trials on the basis of the nature of the target disease and target population. For drugs marketed in Japan, there is a need to include sufficient numbers of Japanese patients in the trials.**

WHAT IS KNOWN AND OBJECTIVE

The rate of successful new drug development has been stagnant over recent years. Only a small portion of all drugs (current success rate, 4%; maximum possible success rate, 19%) that entered phase 1 trials between 1999 and 2004 were finally approved by the US Food and Drug Administration by June 2009.[1] The corresponding success rate in Japan between 2000 and 2008 was estimated to be 44%.[2] The probability of successful transition from phase 1 trial to entry in the market seemed to be higher in Japan than in other regions (i.e. the United States and the European Union). A delay in clinical development in Japan compared with that in the other countries may be a reason for this difference.[3–7]

Correspondence: Ryuta Asada, Department of Experimental Therapeutics Translational Research Center, Kyoto University Hospital, 54 Shogoin Kawahara-cho, Sakyo-ku, Kyoto 606-8507, Japan. Tel.: 81 75 751 4721; fax: 81 75 751 4819; e-mail: rasada@kuhp.kyoto-u.ac.jp

The delay in clinical development in follow-on regions, including Japan, has several advantages in that it enables developers in the follow-on regions to use results of previous clinical trials in foreign countries and to take into account the foreign development process and decisions made by the different regulatory authorities.

The probability of successful transition from each clinical stage of drug development (i.e. phase 1, phase 2, phase 3 and submission) into the market increases as the drug progresses to the subsequent stages.[8] However, a small proportion of submitted new drug applications (NDAs) still fail to be approved by the regulatory authorities.[1,8,9] In Japan, 58 (9·0%) of the 643 NDAs filed between 2004 and 2010 were withdrawn.[10]

Information on the reasons for failure to gain approval may help improve the design of clinical trials and the clinical data package submitted in support of the application of future drugs and thereby improve their success rate and reduce the time required for their development. However, obtaining detailed information about these drugs is extremely difficult because the information about the causes of failure of drug development is almost never disclosed.

To date, several studies have focused on drug development failures and reported reasons such as lack of efficacy, safety concerns and commercial problems.[9,11–13] However, to our knowledge, no studies have examined the detailed reasons why the efficacy of drugs was not shown in clinical trials or the details about the safety concerns.

In this study, we focused on the drugs that had initially failed clinical development but were subsequently approved, that is, we studied the drugs for which the approval application was withdrawn or some of the 'proposed indications and usage' or 'proposed dosage and administration' in the application were not initially approved by the Japanese regulators. Their subsequent approval required remedial action (e.g. undertaking an additional clinical trial). The information about these drugs is available on the official website of the Pharmaceuticals and Medical Devices Agency (PMDA).[14]

The purpose of this study was to analyse th information about these drugs in detail and to discuss critical issues to help optimize drug development.

METHODS

We investigated all NDAs (including supplemental NDA) approved in Japan between April 2001 and March 2011 on the basis of review papers and summary of registration documents, which could be accessed from the official website of PMDA. Of all

NDAs, we identified some NDAs that were withdrawn or in which some of 'proposed indications and usage' or 'dosage and administration' were deleted because of the PMDA reviews, and subsequently, another application was filed after necessary actions were taken, and the application was finally approved. We examined the reasons for withdrawal of these NDAs and deletion of some indications in these NDAs.

RESULTS AND DISCUSSION

Of 727 NDAs approved in Japan between April 2001 and March 2011, 53 were rejected at least once in the review process, but were finally approved. The main reasons for withdrawal of an NDA or rejection of some 'proposed indications and usage' or 'proposed dosage and administration' in the NDA are shown in Table 1. The major reason of the 53 NDAs was 'problem related to clinical data' and accounted for 81% (43 NDAs).

Investigation of NDAs classified into 'problem related to clinical data'

We analysed the 43 NDAs with failures that were categorized as 'problem related to clinical data'. Of these 43 NDAs, the NDAs for clozapine and bepridil hydrochloride hydrate were withdrawn twice, and they were counted as two NDAs. The NDA for loratadine was also counted as two NDAs because a dose-finding trial and a confirmatory trial for each approved indication (i.e. allergic rhinitis and urticaria) of loratadine were simultaneously requested in one NDA review. We closely examined the 46 NDAs and classified them into five categories according to detailed reasons in the light of 'points to be considered by the review staff involved in the evaluation process of a new drug' in Japan.[15] The five categories and the number of NDAs classified under each category are shown in Table 2.

The target diseases for the 46 NDAs classified under the category of 'problem related to clinical data' are shown in Table 3. No significant difference was observed in the numbers of NDAs by therapeutic area, but cancer and cardiovascular diseases were the most popular targets followed by infectious diseases, central nervous system diseases, metabolic diseases and allergic diseases. The proportion of all the approved drugs for these target diseases from 2004 to 2010 was 14%, 7%, 13%, 6%, 17% and 2%, respectively.[16]

Twelve NDAs classified under category A and 16 NDAs classified under category B are further examined in the following section, the details of these NDAs are shown in Table S1.

Eleven NDAs classified under category C were withdrawn because of the violation of Good Clinical Practice (GCP) (7/11) and defective submitted documentation (4/11). Subsequently, additional clinical trials were conducted under GCP or the submitted documents were corrected.

Three NDAs were classified under category D. For botulinum toxin type A, it was necessary to examine the safety of this drug carefully because two cases of death were recognized in the clinical trial in patients with spasmodic torticollis. Subsequently, the clinical trial was performed to examine the minimal effective dose. For clozapine, the development was suspended due to the reports of agranulocytosis in patients with schizophrenia from overseas. Later, focus was placed on the efficacy of clozapine in patients with treatment-resistant schizophrenia, and the additional clinical trial in these patients was conducted. For temsirolimus, it was necessary to examine the result of phase 2 trial carefully because the incidence rate of interstitial pneumonia in Japanese patients tended to be high in the trial. Subsequently, another application was filed after the result of phase 2 trial was investigated minutely.

Four NDAs were classified under category E. For three of those NDAs (human-activated protein C, bepridil hydrochloride hydrate and repaglinide), the development was initiated again after the intended indication and usage were altered. For another product (ketoprofen), the PMDA judged that tapes without cooling effect should be used for treatment of chronic diseases rather than for acute diseases. But the development of ketoprofen tape for treatment of muscle pain was re-initiated as other drug tapes were approved and ketoprofen tape was being used off-label.

Table 1. Main reasons for withdrawal of new drug application (NDA) or rejection of 'proposed indications and usage' or 'proposed dosage and administration'

Main reason	Number of NDAs (%)
Problem related to clinical data	43 (81)
Change of application category	5 (9)
Problem related to CMC/non-clinical data	2 (4)
Unknown	3 (6)
Total	53 (100)

Change of application category: for example, an NDA for indication 'B' was filed under the category of 'new active ingredients' during the regulatory review of a previous NDA of the same drug for another indication 'A'. Thus, the application for indication 'B' has to be withdrawn and resubmitted under the category 'new indication' after the application for indication A was approved.
Unknown: review reports did not have sufficient descriptions, and we were unable to determine exact reasons.
CMC, chemistry, manufacturing and control; NDA, new drug application.

NDA profiles classified into category A (strategic and data package problems)

For the 12 NDAs classified as category A, we analysed the reasons why the NDAs were withdrawn or why some of the 'proposed indications and usage' or 'proposed dosage and administration' in the NDA were deleted. We categorized these reasons into two groups: category A1, 'The data package was inappropriate', and category A2, 'The clinical study design was inappropriate'. Most of the NDAs were categorized into the former group (Table 4).

The details of the NDAs classified under the category A1 were as follows. For five NDAs (oseltamivir phosphate [2004 and 2009 approved], rocuronium bromide, candesartan cilexetil/hydrochlorothiazide combination and somatropin [genetic recombinant drug]), it was necessary to perform a confirmatory trial in Japan because the bridging strategy was inappropriate or unsuccessful. For two NDAs (azithromycin hydrate and basiliximab [genetic recombinant drug]), the Japanese clinical trials for the target disease were not undertaken. For one product (biapenem), the sample size in the Japanese clinical trial was too small for the intended indications. For one product (clozapine), it was necessary to perform a clinical trial to confirm that the patient monitoring system for minimizing the risks in the event of agranulocytosis can be operated successfully in general hospitals and dedicated psychiatric hospitals. For another product (nogitecan hydrochlo-

Table 2. New drug applications classified as 'problem related to clinical data'

Category	Detailed reason	Number of NDAs (%)
A	The development strategy, data package and study designs were not in line with the intended indications and usage	12 (26)
B	The rationale for selecting the dosage regimen was unclear or the efficacy was not confirmed according to the results of the clinical trials	16 (35)
C	The reliability of the data in the submitted documents was not ensured	11 (24)
D	Incidence of serious adverse events	3 (7)
E	The clinical usefulness was unclear	4 (9)
Total		46 (100)

NDA, new drug application.

ride), the PMDA judged that an additional clinical trial was necessary to evaluate efficacy with a valid endpoint.

Most of the NDAs categorized under category A1 were withdrawn because of unsuccessful bridging strategy (5/10). Therefore, information of the cases of unsuccessful bridging strategy should continue to be collected, and the reasons for failure of the bridging strategies should be examined. These results suggest that when a bridging strategy is being planned, it is important to design an adequately planned and well-organized bridging study and to take account of the successful bridging strategy of drugs already approved.[17] In addition, when a clinical data package is being created, it is important to consider the kind of clinical study design necessary and the number of patients required in line with the intended indications and usage.

Two NDAs were classified as category A2. For one product (maxacalcitol), it was necessary to perform a controlled trial that took account of the characteristics, number of patients and age predilection of the target disease. Only unblinded studies without a control were performed at the time of first submission. For another product (tegafur/gimeracil/oteracil potassium combination), the PMDA judged that the clinical study was inappropriate for evaluating the efficacy because the inclusion criteria were inappropriate.

These results suggest that while designing a clinical study, it is important to take account of the nature of the target disease, the number of patients and the development strategy of drugs already approved for a similar indication.

NDA profiles classified into category B (insufficient rationale)

Sixteen NDAs were classified as category B. These NDAs were grouped into one or two categories B1–B3 (Table 5) on the basis of: 'B1, deficiency in the evidence for an optimal dosage regimen' (12 NDAs); 'B2, deficiency in the evidence for the maximum dose' (two NDAs, vardenafil hydrochloride hydrate and irbesartan); and 'B3, efficacy not confirmed in a confirmatory trial' (seven NDAs). Of the seven NDAs classified into category B3, five NDAs were classified into category B1 and B3, and two NDAs (pronase and cetirizine hydrochloride) into only category B3. These results indicated that there often was difficulty in establishing appropriate evidence for the proposed dosage regimen.

Six NDAs were classified as category B1. For sumatriptan succinate and bepotastine besilate, the PMDA judged that the results of dose–response study in the phase 2 trial with multiple-dose regimens were unclear. Each applicant conducted an additional trial with multiple-dose regimens to examine the dose–response. For flecainide acetate and bepridil hydrochloride hydrate, the design of the dose-finding study with multiple-dose regimens was inappropriate (e.g. non-blinded, dose escalation design). For each drug, an additional trial with multiple-dose regimens was conducted using a double-blinded, parallel study design. For pirfenidone, the evidence supporting the efficacy was deficiency in the result of a phase 2 study with a single-dose regimen, and so, an additional trial with multiple-dose regimens was conducted. For tacrolimus hydrate, the validity of the methods used for dose adjustment in the phase 2 study with multiple-dose regimens was not sufficient. A phase 3 study was not conducted. So an additional trial with a single-dose regimen was conducted to confirm the suitability of the proposed novel method for dose adjustment. For febuxostat, the PMDA concluded that further examination of the optimal dose and method of administration was necessary because of the occurrence of adverse events, and then an additional trial with multiple-dose regimens was conducted.

Five NDAs were subclassified as categories B1 and B3. For loratadine (indication for allergic rhinitis and urticaria), the result of a dose–response study in the phase 2 trial with multiple-dose regimens was unclear, and the design of a phase 3 study was

Table 3. Target diseases for the 46 NDAs identified under the category 'problem related to clinical data'

Target disease	Number of NDAs (%)					
	Category A–E	Category A	Category B	Category C	Category D	Category E
Cancer	7 (15)	2	0	4	0	1
Cardiovascular diseases	7 (15)	1	5	1	0	0
Infectious diseases	6 (13)	4	0	2	0	0
Central nervous system diseases	5 (11)	2	2	1	0	0
Metabolic diseases	4 (9)	0	3	0	0	1
Allergic diseases	4 (9)	0	4	0	0	0
Other	13 (28)	3	2	3	3	2
Total	46 (100)	12	16	11	3	4

Table 4. Detailed reasons for classification of the NDAs as category A

Category	Detailed reason	Number of NDAs
A1	The clinical data package was inappropriate	10
A2	The clinical study design was inappropriate	2

NDA, new drug application.

Table 5. Detailed reasons for classification of the NDAs as category B

Category	Detailed reason	Number of NDAs
B1	Deficiency in the evidence of an optimal dosage regimen	12
B2	Deficiency in the evidence of maximum dose	2
B3	Efficacy was not confirmed in a confirmatory trial	7

NDA, new drug application.

Table 6. Main changes in the additional clinical study undertaken

Changes in clinical study	Numbers (%)
Study design	3 (6)
Change from crossover design to parallel group design	1
Change from unblinded trial to double-blind trial	2
Study subjects	4 (9)
Limitation of study subjects	2
Alteration of study target disease	2
Dosage regimen	11 (23)
Addition of criteria for taking medicine	1
Increase of dose in a confirmatory trial	3
Addition of a low-dose group	3
Addition of a high-dose group	1
Alteration of dose escalation method	2
Alteration of dose adjustment method	1
Duration of exposure	4 (9)
Extension of duration	3
Shortening of duration	1
Control group	13 (28)
Addition of placebo group (include pseudo-placebo)	8
Alteration of control drug	4
Addition of control drug	1
Endpoint	12 (26)
Alteration of primary endpoint	9
Alteration of methods to evaluate efficacy	3
Total	47 (100)

inappropriate. An additional trial was conducted to confirm superiority over placebo (or pseudo-placebo) and non-inferiority against an existing drug. For lansoprazole and celecoxib, non-inferiority was confirmed against an existing drug in the confirmatory trial. For duloxetine hydrochloride, the dose determined in the clinical studies (under 30 mg) was inappropriate. In the cases of lansoprazole, celecoxib and duloxetine hydrochloride, additional clinical trials were conducted to confirm the efficacy with higher doses than used in the clinical trials reported in the initial NDA. These results showed that it was necessary to carefully determine the dosage regimen in clinical trials to include the starting dose, the dose titration method and the maximum dose. All available information should be analysed when a clinical trial is planned.

In all the NDAs identified as category B, additional clinical studies were performed to obtain the approval after the initial application was withdrawn or after some 'proposed indications and usage' or 'proposed dosage and administration' in this application were removed. When the trial sponsors designed these additional studies, it was possible to consider points raised in the regulatory review. Thus, the study designs were more likely to be appropriate. Therefore, we compared the designs of these studies in the latter application with those of the studies in the initial application.

Changes to the initial studies made in the additional clinical studies are shown in Table 6. Changes relating to 'control group' were most common (28%) followed by 'endpoint' (26%) and 'dosage regimens' (23%).

Of the changes relating to 'control group', 'addition of placebo group' was the most common (8/13). This might be attributed to the timing of clinical studies that were submitted in the initial NDAs with most of these studies being performed before 2000. In Japan, placebo-controlled clinical trials were not performed actively before 2000 because of concerns about the ethics of such trials.[18] However, the International Conference on Harmonization of Technical Requirements for Registration of Pharmaceuticals for Human Use (ICH) E10 guideline[19] was issued in 2001 and use of placebo gradually became more common for certain circumstances.[18] Therefore, setting a placebo group is unlikely to be a problem at present because of the E10 guideline, and control groups were set appropriately in these trials.

Among the actions related to 'endpoint', there were problems with 'alteration of primary endpoint' (9/12) and 'alteration of methods to evaluate efficacy' (3/12). The latter was also related to the primary endpoint. Most of the remedial actions related to changes in primary endpoint to allow more objective evaluation of outcome. These observations suggest that it is important to ensure that the methods used allowed objective evaluation of efficacy.

WHAT IS NEW AND CONCLUSION

Our results indicate the importance of careful determination of the optimal dosage regimen and the choice of objective endpoints in clinical trials. Further, it is important to establish a clear strategy for generating the clinical data package, to include careful design of clinical trials on the basis of the nature of the target disease and target population. For drugs marketed in Japan, there is a need to include sufficient numbers of Japanese patients in the trials. We recommend that regulatory authorities be consulted early to identify likely problems.

SUPPORTING INFORMATION

Additional Supporting Information may be found in the online version of this article:

Table S1. Details of the NDAs classified into Category A and B.

REFERENCES

1. DiMasi JA, Feldman L, Seckler A, Wilson A. Trends in risks associated with new drug development: success rates for investigational drugs. *Clin Pharmacol Ther*, 2010;**87**:272–277.
2. Yagi T, Ohkubo M, Ono S. Times and cost of new drug development – a survey through questionnaire. 2010. (No. 29, Seisakuken News, Office of Pharmaceutical Industry Research) (In Japanese).
3. Ishibashi K. Investigation of drug lag in Japan – current trends and issues based on questionnaire to pharmaceutical companies. 2008. (No. 40, Research Paper Series, Office of Pharmaceutical Industry Research) (In Japanese).
4. Hirai Y, Yamanaka Y, Kusama M, Ishibashi T, Sugiyama Y, Ono S. Analysis of the success rates of new drug development in Japan and the lag behind the US. *Health Policy*, 2012;**104**:241–246.
5. Ishibashi T, Kusama M, Sugiyama Y, Ono S. Analysis of regulatory review times of new drugs in Japan: association with characteristics of new drug applications, regulatory agency, and pharmaceutical companies. *J Clin Pharm Ther*, 2012;**37**:657–663.
6. Tsuji K, Tsutani K. Approval of new drugs 1999–2007: comparison of the US, the EU and Japan situations. *J Clin Pharm Ther*, 2010;**35**:289–301.
7. Shimazawa R, Kusumi I, Ikeda M. Delays in psychiatric drug development in Japan. *J Clin Pharm Ther*, 2012;**37**:348–351.
8. Arrowsmith J. A decade of change. *Nat Rev Drug Discov*, 2012;**11**:17.
9. Kola I, Landis J. Can the pharmaceutical industry reduce attrition rates? *Nat Rev Drug Discov*, 2004;**3**:711–715.
10. Pharmaceuticals and Medical Devices Agency, Japan. Annual Report FY2010. 2011. Available at: http://www.pmda.go.jp/english/about/pdf/2010/annual_report_FY2010.pdf (accessed 30 March 2012).
11. DiMasi JA. Risks in new drug development: approval success rates for investigational drugs. *Clin Pharmacol Ther*, 2001;**69**:297–307.
12. Arrowsmith J. Trial watch: Phase 2 failures: 2008–2010. *Nat Rev Drug Discov*, 2011;**10**:328–329.
13. Arrowsmith J. Trial watch: Phase 3 and submission failures: 2007–2010. *Nat Rev Drug Discov*, 2011;**10**:87.
14. Official web-site of the Pharmaceuticals and Medical Devices Agency. Available at: http://www.info.pmda.go.jp/info/syounin_index.html (accessed 30 March 2012) (In Japanese).
15. Pharmaceuticals and Medical Devices Agency, Japan. Points to be considered by the review staff involved in the evaluation process of new drug. Available at: http://www.pmda.go.jp/english/service/pdf/points.pdf (accessed 17 April 2008).
16. Fukuhima T, Ono S. Performance of clinical development and approval review of new drugs in Japan – approved NDAs between 2000–2010. 2011. (No. 51, Research Paper Series, Office of Pharmaceutical Industry Research) (In Japanese).
17. Uyama Y, Shibata T, Nagai N, Hanaoka H, Toyoshima S, Mori K. Successful bridging strategy based on ICH E5 guideline for drugs approved in Japan. *Clin Pharmacol Ther*, 2005;**78**:102–113.
18. Ogaki T, Fujino A. Ethical consideration on the validity of placebo control groups in clinical trials. *J Jpn Assoc Bioethics*, 2010;**20**:38–46. (In Japanese).
19. International Conference on Harmonisation. CHOICE OF CONTROL GROUP AND RELATED ISSUES IN CLINICAL TRIALS: E10. Available at: www.ich.org/fileadmin/Public_Web_Site/ICH…/E10/…/E10_Guideline.pdf (accessed 20 July 2000).

Biochimica et Biophysica Acta 1830 (2013) 4046–4052

Contents lists available at SciVerse ScienceDirect

Biochimica et Biophysica Acta

journal homepage: www.elsevier.com/locate/bbagen

Evasion from accelerated blood clearance of nanocarrier named as "Lactosome" induced by excessive administration of Lactosome

Eri Hara [a], Akira Makino [b], Kensuke Kurihara [c], Manabu Sugai [a], Akira Shimizu [a], Isao Hara [d], Eiichi Ozeki [d], Shunsaku Kimura [e,*]

[a] Department of Experimental Therapeutics, Translational Research Center, Kyoto University Hospital, Kyoto, 606-8507, Japan
[b] Division of Molecular Imaging, Biomedical Imaging Research Center, University of Fukui, Fukui, 910-1193, Japan
[c] Clinical Division of Diagnostic Radiology, Kyoto University Hospital, Kyoto, 606-8507, Japan
[d] Technology Research Laboratory, Shimadzu Corporation, Kyoto, 619-0237, Japan
[e] Department of Material Chemistry, Graduate School of Engineering, Kyoto University, Kyoto, 615-8510, Japan

ARTICLE INFO

Article history:
Received 18 January 2013
Received in revised form 17 March 2013
Accepted 20 March 2013
Available online 29 March 2013

Keywords:
Molecular imaging
Nanoparticle
ABC phenomenon
Immune tolerance

ABSTRACT

Background: Nanoparticle of Lactosome, which is composed of poly(L-lactic acid)-base depsipeptide with diameter of 35 nm, accumulates in solid tumors by the enhanced permeability and retention (EPR) effect. However, a pharmacokinetic alteration of Lactosome was observed when Lactosome was repeatedly administered. This phenomenon is named as the Lactosome accelerated blood clearance (ABC) phenomenon. In this study, the effect of Lactosome dose on the ABC phenomenon was examined and discussed in terms of immune tolerance.
Methods: To tumor transplanted mice, Lactosome (0–350 mg/kg) was administrated. At 7 days after the first administration, indocyanine green (ICG)-labeled Lactosome (ICG-Lactosome, 0–350 mg/kg) was injected. Near-infrared fluorescence imaging was performed, and biodistribution of ICG-Lactosome was evaluated. Further, the produced amounts of anti-Lactosome IgM were determined by enzyme-linked immunosorbent assay (ELISA).
Results: ICG-Lactosome accumulated in the tumor region when the first Lactosome dose exceeded over 150 mg/kg. The amounts of anti-Lactosome IgM were inversely correlated with the first Lactosome doses. Even after establishment of the Lactosome ABC phenomenon with the first Lactosome dose as low as 5.0 mg/kg, the Lactosome ABC phenomenon can be evaded apparently by dosing ICG-Lactosome over 50 mg/kg regardless of anti-Lactosome IgM production.
Conclusions: There are two different mechanisms for evasion from the Lactosome ABC phenomenon before and after its establishment. In either mechanism, however, the Lactosome ABC phenomenon can be evaded by excessive administration of Lactosome.
General significance: Lactosome is a potential nanocarrier for drug and/or imaging agent delivery, which can be used for frequent administrations without significant pharmacokinetic alterations.

1. Introduction

Application of nanoparticles for chemotherapy has been actively investigated on possible control of biodistribution and blood circulation behavior of drugs through their encapsulation into nanoparticles [1,2]. For example, the applications of nanoparticles for the tumor targeted drug delivery of anticancer drugs is actively investigated utilizing phenomenon that nanoparticles are selectively accumulated into solid tumor regions by the enhanced permeability and retention (EPR) effect [3,4].

Lactosome is a polymeric micelle with ca. 35 nm diameter, which is composed of amphiphilic block polydepsipeptide, poly(sarcosine)-*block*-poly(L-lactic acid) [5]. The average block sizes of hydrophilic poly(sarcosine) and hydrophobic poly(L-lactic acid) were 60–90mer and 30mer, respectively. Lactosome shows a long blood circulation behavior and Lactosome labeled with indocyanine green (ICG-Lactosome) successfully imaged tumor orthotopically implanted on liver, which is due to suppression of non-tumor associated capture of Lactosome by liver. The high contrast imaging of tumors in liver becomes possible due to the contribution of hydrophilic poly(sarcosine) chains covering the surface of Lactosome densely in a polymer brush state. However, the biodistribution of Lactosome at the second dose was changed to show a rapid clearance from the blood stream by entrapment in liver [6]. This drastic pharmacokinetic alteration is caused by productions of anti-Lactosome IgM and anti-Lactosome IgG_3 after first administration of Lactosome, because Lactosome induced the T-cell independent (TI) B cell immune response. The similar pharmacokinetic alteration was also observed with PEGylated liposome, which is called as the accelerated blood clearance (ABC) phenomenon [7–10]. The ABC

* Corresponding author. Tel.: +81 75 383 2400; fax: +81 75 383 2401.
E-mail address: shun@scl.kyoto-u.ac.jp (S. Kimura).

0304-4165/$ – see front matter © 2013 Elsevier B.V. All rights reserved.
http://dx.doi.org/10.1016/j.bbagen.2013.03.024